Acta Biomaterialia 102 (2020) 83–99

Contents lists available at ScienceDirect

Acta Biomaterialia

journal homepage: www.elsevier.com/locate/actbio

Full length article

# Biomechanical and microstructural characterisation of the porcine stomach wall: Location- and layer-dependent investigations

Melanie Bauer[a], Enrique Morales-Orcajo[a], Lisa Klemm[a], Robert Seydewitz[a], Victoria Fiebach[a], Tobias Siebert[b], Markus Böl[a,*]

[a] Institute of Solid Mechanics, Technische Universität Braunschweig, Braunschweig D-38106, Germany
[b] Institute of Sport and Motion Science, University of Stuttgart, Stuttgart D-70569, Germany

ARTICLE INFO

*Article history:*
Received 30 August 2019
Revised 19 November 2019
Accepted 19 November 2019
Available online 22 November 2019

*Keywords:*
Stomach wall
Biaxial tension testing
Tissue composition
Microstructure
Smooth muscle
Tissue staining

ABSTRACT

The mechanical properties of the stomach wall help to explain its function of storing, mixing, and emptying in health and disease. However, much remains unknown about its mechanical properties, especially regarding regional heterogeneities and wall microstructure. Consequently, the present study aimed to assess regional differences in the mechanical properties and microstructure of the stomach wall. In general, the stomach wall and the different tissue layers exhibited a nonlinear stress-stretch relationship. Regional differences were found in the mechanical response and the microstructure. The highest stresses of the entire stomach wall in longitudinal direction were found in the corpus (201.5 kPa), where food is ground followed by the antrum (73.1 kPa) and the fundus (26.6 kPa). In contrast, the maximum stresses in circumferential direction were 39.7 kPa, 26.2 kPa, and 15.7 kPa for the antrum, fundus, and corpus, respectively. Independent of the fibre orientation and with respect to the biaxial loading direction, partially clear anisotropic responses were detected in the intact wall and the muscular layer. In contrast, the innermost mucosal layer featured isotropic mechanical characteristics. Pronounced layers of circumferential and longitudinal muscle fibres were found in the fundus only, whereas corpus and antrum contained almost exclusively circumferential orientated muscle fibres. This specific stomach structure mirrors functional differences in the fundus as well as corpus and antrum. Within this study, the load transfer mechanisms, connected with these wavy layers but also in total with the stomach wall's microstructure, are discussed.

**Statement of significance**

This article examines for the first time the layer-specific mechanical and histological properties of the stomach wall attending to the location of the sample. Moreover, both mechanical behaviour and microstructure were explicitly match identifying the heterogeneous characteristics of the stomach. On the one hand, the results of this study contribute to the understanding of stomach mechanics and thus to their functional understanding of stomach motility. On the other hand, they are relevant to the fields of constitutive formulation of stomach tissue, whole stomach mechanics, and stomach-derived scaffolds i.e., tissue-engineering grafts.



## 1. Introduction

With more than one million new cases in 2018, stomach cancer is the fifth common estimated cancer worldwide, leading to 782,685 deaths and representing the second leading cause of cancer death [16]. In women, the rate is half as high as in men. Among men, in several Western Asian countries, it is the most commonly diagnosed cancer and the leading cause of cancer death. While the incidence rates in North America and Northern Europe are low, they have increased significantly in recent years.

Gastrectomy, the partial or total surgical removal of the stomach, has become a reliable intervention for achieving complete removal of the tumour lesion. Despite its healing potential, complications, mostly attributed to the limited capacity for food intake and the lack of various glands, remain a common clinical problem

* Corresponding author.
*E-mail address:* m.boel@tu-bs.de (M. Böl).

https://doi.org/10.1016/j.actbio.2019.11.038
1742-7061/© 2019 Published by Elsevier Ltd on behalf of Acta Materialia Inc.

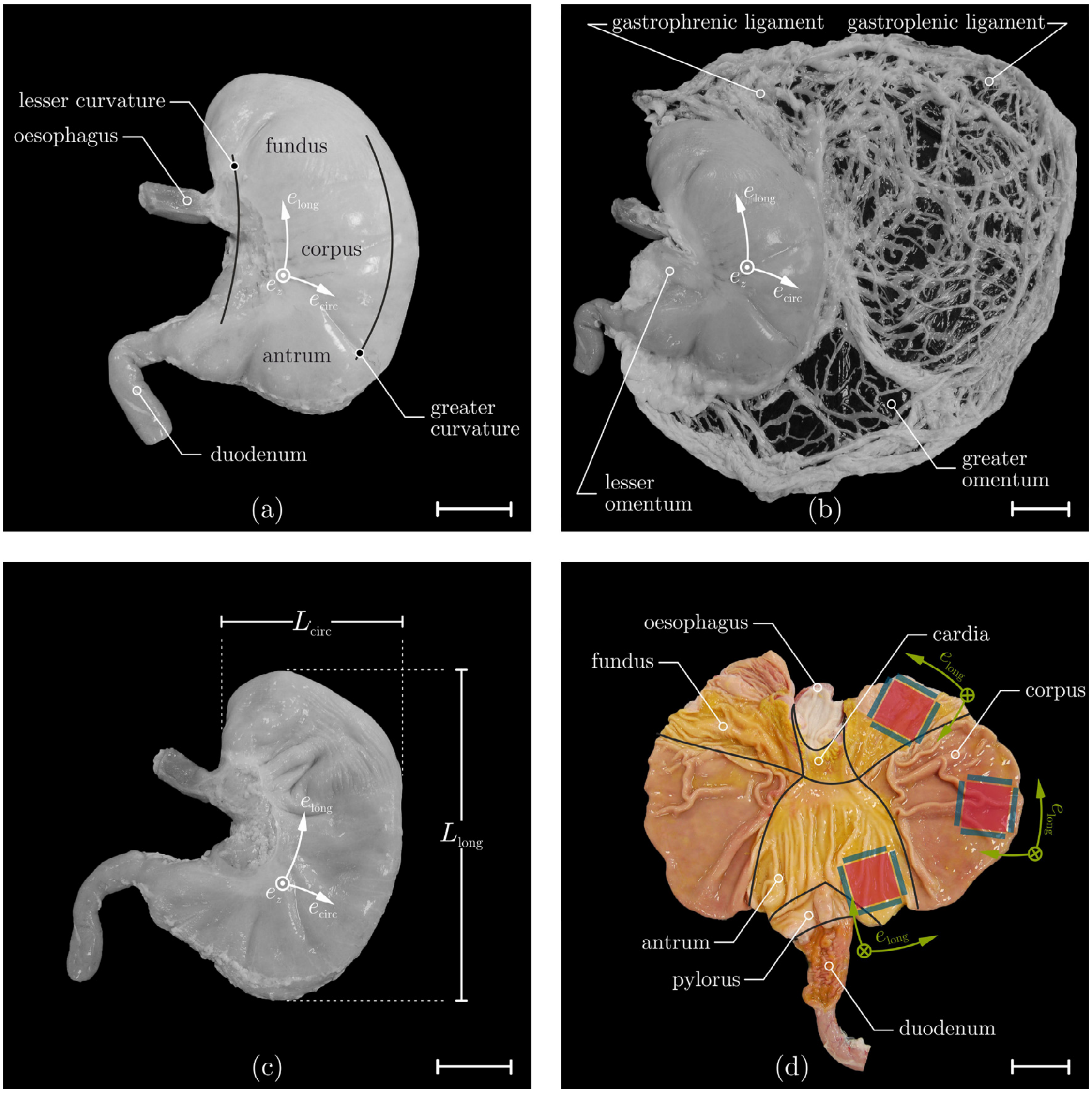


**Fig. 1.** Porcine stomach anatomy and tissue sample dissection. Stomach inflated with physiological solution featuring (a) without and (b) with extended ligaments. (c) Exterior view of a deflated stomach allowing the measurements of projected gross dimensions Llong and Lcirc. (d) Interior view of a stomach opened along the greater curvature. Here, the original colours are presented, allowing optical differentiation of the various regions. Samples for mechanical and histological investigations are coloured in red and blue, respectively. Note, the orientation of the mechanical samples is oriented in the longitudinal direction (i.e., parallel to the greater curvature), cf. green coordinate systems. Scale bars: 5 cm. (For interpretation of the references to color in this figure legend, the reader is referred to the web version of this article.)

[e.g. 13,18,20,46], which is accompanied by a marked reduction in the quality of life. To improve the quality of life, various gastric replacement techniques have been developed, whereby, based on its technical ease, the Roux-en-Y technique is the most common [1,9]. However, a criticism of all these techniques is the subsequent limited capacity for food intake. Therefore, a tissue engineered stomach may represent an alternative approach to replacing the mechanical and metabolic functions of the normal stomach [e.g. 25,43–46]. Consequently, ideal materials for partial or complete stomach replacement in the sense of tissue engineering should possess biological compatibility and mechanical reliability [e.g. 5,27,28,46,59]. To design appropriate surgical repair procedures and develop materials for stomach reconstruction, it is necessary to fully understand the mechanical characteristics of the normal, healthy stomach at different scales. Thereby, the correlation of tissue mechanical quantities with those at the microstructural level will aid in understanding load transfer mechanisms taking place inside the stomach wall.

The stomach, part of the gastrointestinal tract, is a J-shaped distensible organ located between the oesophagus (proximal) and the duodenum (distal). It has three main functions [26,48]: First, to act as a reservoir for ingested food received from the oesophagus; second, to grind the bolus and blend it with gastric secretions, resulting in chyme; and third, to control the release of chyme into the duodenum for proper digestion and absorption. During this process, the stomach is subjected to large deformations [32,41,58,65]. To accomplish these tasks, from the gross anatomical viewpoint, the stomach is divided into three main regions (from proximal to distal), see Fig. 1: Fundus, corpus, and antrum. Additionally, there are two regions around the inlet and outlet orifices, the cardia and the pylorus, respectively. The sizes of these regions vary greatly between individuals and ages. Further, the transition between them is gradually revealing mixed features [55].

From the mechanical point of view, the stomach wall (SW) has remarkable characteristics that are responsible for the functionality of the stomach. Essential for this is the microstructure of the

SW, which consists of four layers (from inside out), see Fig. 7: Mucosal, submucosal, muscular, and serosal layer. Mechanically, the mucosal layer and the muscular layer are the most relevant. The mucosal layer, consisting of the tunica mucosa and tela muscularis mucosa, exhibits, depending on the regions of the stomach, prominent folds. The submucosal layer, consisting of the tela submucosa, separates the mucosal layer from the muscular layer, making the mucosal layer independent of the contractile state of the muscular layer [42,55]. The muscular layer itself is composed of smooth muscle cells (SMCs), forming smooth muscle fibres, which are embedded in a collagenous extracellular matrix (ECM) arranged in at least two layers of different fibre orientations, namely, the stratum circulare and stratum longitudinale [12,15,19]. Thereby, the outer layer (stratum longitudinale) runs continuous, following the longitudinal fibres of the oesophagus. The inner layer (stratum circulare) is best developed in the pylorus (distal part of the antrum). Its presence in the cardia is controversial. Based on single analyses [3,29,55,64], there exists a third layer characterised by obliquely oriented fibres, which is incomplete and more evident in the cardia [3,29,55,64], see Fig. 7. Finally, the serosal layer, consisting of the tunica serosa, comprises the outermost layer. However, depending on the position within the SW, all layers vary significantly in their geometrical, morphological, and microstructural characteristics, i.e., in thickness, waviness, and orientation.

For a comprehensive understanding of the stomach's passive function, especially in terms of tissue engineering, experimental investigations are indispensable. Generally, there exist few studies that can be grouped into two types: The first focuses on whole organ experiments, and the second includes axial and biaxial experiments at tissue scale. As the stomach is a sack-like organ, at the organ level, its passive properties have been measured using gastro-dynamic barostat inflation tests [2,7,8,23,50,60] as part of daily clinical practice and without using a gastric barostat [17,22,40,41,65]. While these experiments show that quantities, such as flow rate or pressure, can be easily related to the applied volume, wall tissue properties, e.g., layer-specific characteristics, cannot be directly assessed. In contrast, by performing tissue level experiments on SW strips in the form of axial tension [21,33,63,71,75,76] and compression [62], as well as biaxial tension, experiments [6], more specific characteristics can be elucidated. Utilising position-dependent experiments [6,33,63,75,76], variations in mechanical behaviour can be analysed. Further, due to orientation-dependent axial experiments [21,33,39,63,75,76], anisotropic mechanical characteristics can be studied. Finally, Zhao et al. [76] and Jia et al. [33] studied layer-specific characteristics of the SW. Overall, the SW exhibits viscoelastic, nonlinear, and anisotropic mechanical properties. Therefore, these properties are strongly location-, direction-, and layer-dependent.

Despite these findings, the aforementioned mechanical properties in combination with the SW's underlying microstructure are not yet well understood, especially when focusing on the stomach's function. In addition, the specific (micro)structure of the SW poses large challenges for measuring technique as well. On the one hand, axial tensile experiments cannot adequately reflect in vivo physiological loadings. Thus, this is more likely to be accomplished by performing biaxial experiments. Another challenge is the comparison of the mechanical response of isolated layers and intact SW samples. Since the mucosal layer presents, compared to the muscular layer, large folds in the in vivo state [42,55], it is necessary to determine a common reference state prior to sample excision to achieve a realistic comparison [74].

In summary, no systematic studies have been performed so far that correlate the mechanical properties of each gastric region with its microstructural peculiarities. It has been suggested that changes in soft tissue microstructure lead to changes in the mechanical properties. Changes in these mechanical properties are usually due to changing loading conditions or to adaptation of the tissue to a pathological environment [37]. Therefore, the aim of this study was to deepen the understanding of SW mechanics by relating mechanical response to its microstructure for future tissue engineering approaches.

## 2. Materials and methods

### 2.1. Stomach and sample dissection

The porcine stomachs used within this study were harvested immediately after animal sacrifice from a local slaughterhouse and were transported to the laboratory within 30 minutes. To ensure a passive state, i.e., to prevent spontaneous contraction of the samples during testing, the organs were transported and stored during the entire testing phase in calcium-free Krebs solution composed of [56] 113 mM NaCl, 4.7 mM KCl, 1.2 mM $MgSO_4$, 25 mM $NaHCO_3$, 1.2 mM $KH_2PO_4$, 5.9 mM dextrose, and 1 mM EGTA at 4 °C. Pigs (*Sus scrofa domestica*) were approximately 6 months old and weighed approximately 90 kg. A total of forty-four ($n = 44$) stomachs were used for mechanical and histological analyses. Within the animal body, the stomach is mainly mounted on the lesser and greater omentum, attaching on the lesser and greater curvature, respectively. While the lesser omentum consists of hepatogastric and hepatoduodenal ligaments, the greater omentum encompasses the gastrophrenic, gastrocolic, and gastrosplenic ligaments [67,73], see also Fig. 1(b). Prior to sample preparation, stomachs were emptied and measured in their deflated state. Following Fig. 1(c), the average size of the stomachs was 215.5 ± 21.2 mm and 99.2 ± 11.7 mm in the projected longitudinal $L_{long}$ and circumferential lengths $L_{circ}$, respectively. In the next step, stomachs were opened along the greater curvature and rinsed with running water. In this state, different regions of the stomach, see Fig. 1(d), are clearly distinguishable due to different colours of the gastric rugae. These tissue landmarks were used as references to define sample locations.

### 2.2. Mechanical experiments

For mechanical characterisation of the SW, square samples of 40 mm side length were biaxially tested, depending on the tissue sample location, its specific layers, and fibre orientations. In doing so, experiments were performed on samples taken from the fundus, corpus, and antrum, see also Fig. 1(d). For each of these locations, intact wall samples, samples featuring the muscular layer, and those consisting of the mucosal layer were equibiaxially tested. Finally, for each location and layer, samples oriented parallel to the greater curvature (denoted by 0°) and those rotated by 45° were considered. An additional set of samples, rotated by 22.5°, taken from the corpus was considered for the mechanical tests. In summary, 3 regions, 3 layers, and 2 orientations, alternatively 3 orientations in the corpus, were considered, leading to 21 different cases. Thus, considering a sample number of four ($n = 4$) result in a total number of eighty-four ($n = 84$) samples. As shown in Fig. 1(d), samples were located in the middle of each respective region and oriented with respect to the greater curvature. From each half of an opened stomach, samples symmetrically located and oriented were excised. Samples from the right side were tested intact, and samples from the left side were layer-separated and independently tested. In this way, it was possible to systematically compare the response of the intact wall versus the response of each layer independently for an individual specimen. All samples were tested in the original state, i.e., keeping the natural folding, as explained in Section 2.2.1. In addition, the four sides surrounding the sample, see blue rectangle in Fig. 1(b), were fast-frozen and stored for subsequent histological analyses. All tests were performed within 12 hours of animal sacrifice.

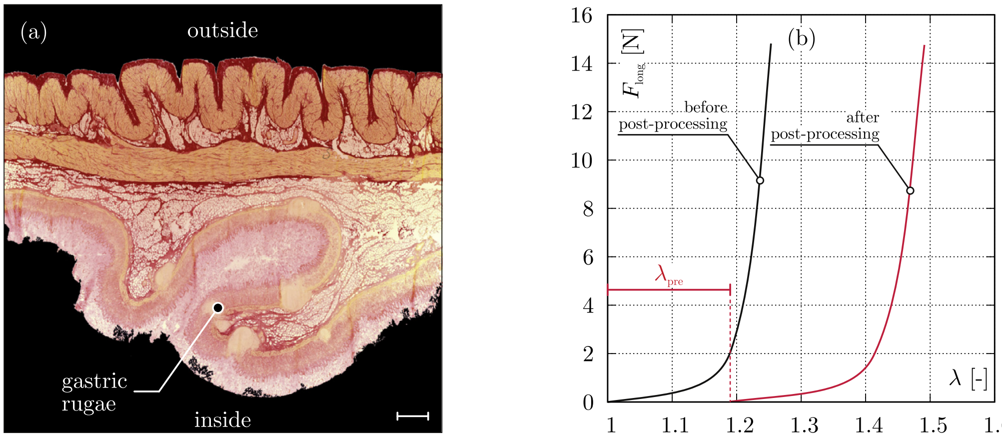


**Fig. 2.** Stomach wall reference state and pre-stretch calculation. (a) Histological crosssection of the porcine SW (fundus) stained with Picro-Sirius red and (b) corresponding raw mechanical force-stretch response (longitudinal direction) of the mucosal layer before (black) and mechanical response after (red) post-processing. Sale bar: 1 mm. (For interpretation of the references to color in this figure legend, the reader is referred to the web version of this article.)

### 2.2.1. *Reference state of the gastric specimen*

In the stomach's deflated state, the muscular layer and the mucosal layer are characterised by clearly pronounced waviness, also called gastric rugae, see Fig. 2(a). By comparing these regions, clear differences in the wave frequencies can be detected, indicating complex load transfer mechanisms during the stomach's daily tasks from a mechanical point of view. However, improper handling during the testing process can result in a specimen's geometry being falsified. Due to its softness, this is especially the case for the mucosal layer when removing it from the SW for mechanical tests. In this situation, the mucosal layer might be elongated and thus, does not reflect its natural waviness as in the in vivo situation, which is defined as the mechanical reference state. Taking this into account, the sampling history was tracked throughout the whole process, from sample excision to final mechanical biaxial testing, by working on a sheet of polystyrene foam on which the sample edges were needled for each step while simultaneously photographing the individual situations. Once the sample location and orientation were determined, a sample pattern with the hook's insertions and marker locations was needled onto the tissue and a perfect 40 mm square sample was excised. For layer-specific experiments, layers were separated at the submucosal layer and mounted on new polystyrene foam sheets, maintaining the sample orientation with respect to the organ axes. Thus, the muscular layer in fact consisted of the muscular and serosal layer and parts of the submucosal layer, while the mucosal layer also included parts of the submucosal layer. For experiments on the entire wall structure, samples were directly hooked onto the polystyrene foam sheet. Up to this point, samples were needled to the polystyrene foam sheet and maintained at the original 40 × 40 mm square shape. An image of the sample at this state was recorded and this configuration, to be the in vivo situation, was defined as the reference state of the specimen, needed for the calculation of the sample's stretching history. Henceforth, pictures of the current state, including the hook and marker positions at each situation, i.e., preparation, mounting, preloading, and testing, were recorded to allow recalculation with respect to the reference state. In doing so, at the beginning of each mechanical test, different stretch histories were determined and considered within the mechanical tests for the intact wall, the muscular layer, and the mucosal layer. For more detailed explanation see Remark 1. Hereafter, the stretch history before the beginning of the mechanical test was referred to as 'pre-stretch' ($\lambda_{\mathrm{pre}}$), see Fig. 2(b), and considered in post-processing analyses.

**Remark 1.** [Layer-specific pre-stretch history determination] During tissue handling the SW as well as the different layers pass through different configurations before actual mechanical testing and which in fact leads to tissue sample elongation in both directions (circumferential and longitudinal). In Fig. 3 this situation is schematically illustrated, exemplarily in one loading direction. Two scenarios have to be considered, first the handling of the entire SW samples (a) to (b) and second the handling of the individual layers, see (a), (c) and (d). In the first case, the sample is dissected from the stomach. This situation features the reference state for the following considerations. Thus, the length of the sample is denoted by $l_0$. During further handling, e.g. in form of mounting and pre-loading the strip becomes lengthened, denoted by $l^{\mathrm{SW}}$, see (b), allowing the determination of the pre-stretch $\lambda_{\mathrm{pre}}^{\mathrm{SW}} = l^{\mathrm{SW}}/l_0$ for the entire SW strip. For the layer-specific experiments, the mucosal layer is separated from the muscular layer. This leads to a moderate elongation of the muscular layer but to a significant lengthening of the mucosal layer, which is mainly due to the unfolding of the wavy structure of the gastric rugae, see (c). Further handling in form of mounting and pre-loading increases the lengths $l^{\mathrm{muco}}$ and $l^{\mathrm{musc}}$ of the two layers, resulting in layer-specific pre-stretches of $\lambda_{\mathrm{pre}}^{\mathrm{muco}} = l^{\mathrm{muco}}/l_0$ and $\lambda_{\mathrm{pre}}^{\mathrm{musc}} = l^{\mathrm{musc}}/l_0$ for the mucosal and muscle layer, respectively, see (d). Due to its softness, but especially because of its wavy structure, which becomes unfolded when separating from the muscular layer, the mucosal layer is characterised by a large amount of pre-stretch, see also Fig. 5.

### 2.2.2. *Biaxial, mechanical testing*

To perform the mechanical, equibiaxial experiments, a planar biaxial testing machine was used, featuring four linear actuators that can be controlled independently by force, position, or stretch. For detailed information, the interested reader is referred to Morales-Orcajo et al. [51]. Briefly, square samples uniformly hooked on all four edges were equibiaxially tested. To accomplish the deformation-controlled experiments, nine markers positioned on a nine-dot grid were glued to the centre of the sample, see Fig. 4(b), allowing in-plane deformation measurement via the video extensometer (recording rate 20 Hz), providing 24-bit images with a resolution of 1280 (horizontal) × 1024 (vertical) pixels (scale: 31.8 pixel/mm) in jpg format, with which the testing machine is equipped. The tracking area of 6 mm edge length constitutes 4% of the area bound by the hooks (30 × 30 mm), ensuring homogeneous stress distribution in the tracking area [70].

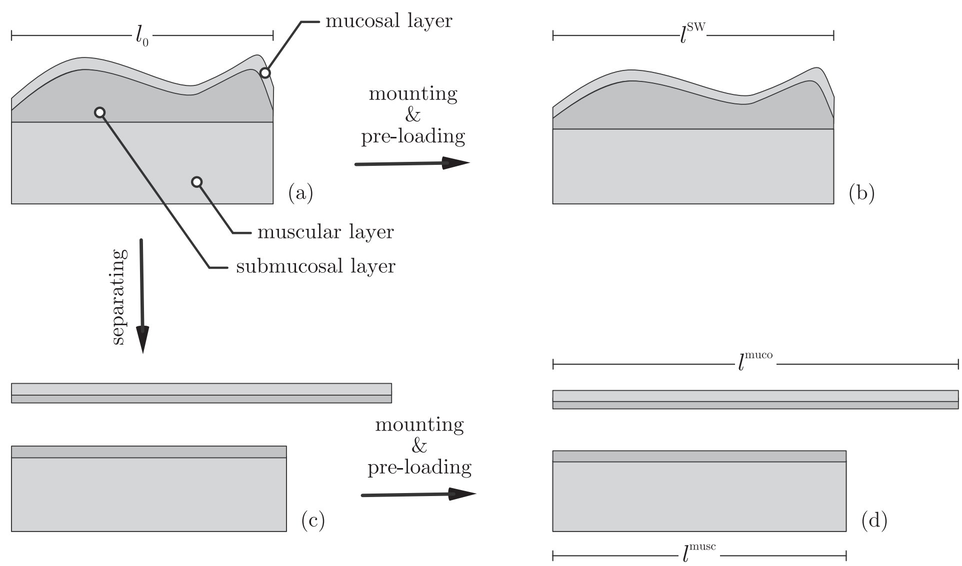


**Fig. 3.** Idealised illustration of the sampling history from sample excision to final mechanical biaxial testing: (a) Entire SW sample, dissected from the organ, (b) elongated sample after mounting and pre-loading, (c) elongated SW layers after separation, and (d) SW layers after additional mounting and pre-loading. Note, only one tissue direction is displayed here for reasons of clarity.

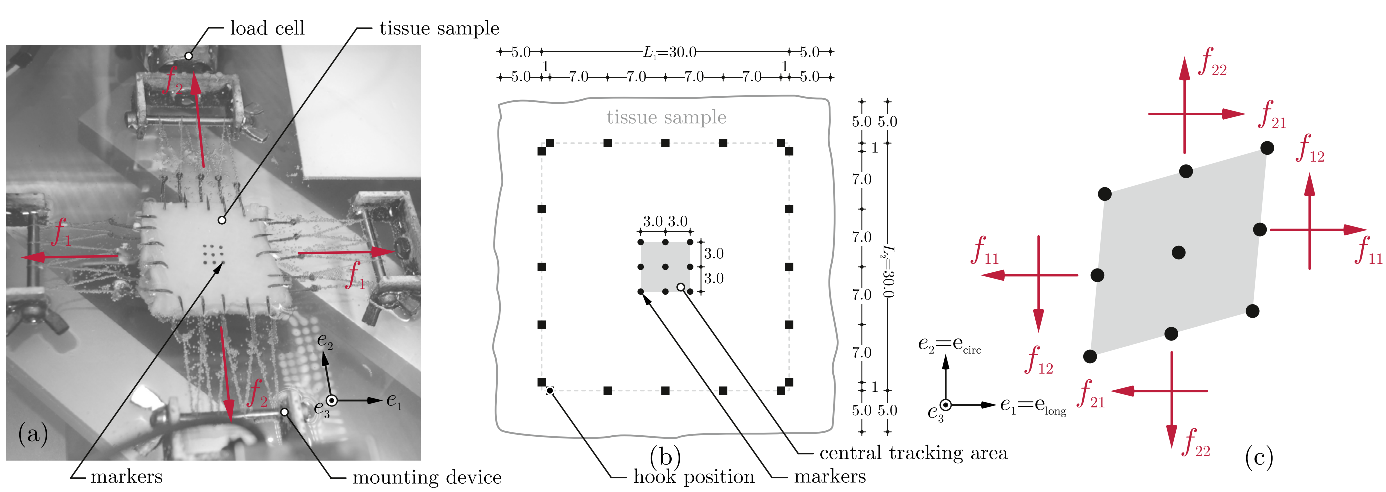


**Fig. 4.** Experimental setup: (a) View of the specimen mounted in the biaxial testing machine, (b) idealised illustration of the marker (filled cycles) and hook (filled squares) positions (dimensions are given in millimetres), and (c) forces acting on the tracked area.

Samples were tested submerged in calcium-free Krebs solution at 37° C bubbled with 95% $O_2$ and 5% $CO_2$.

The test protocol was straightforward: With the sample mounted in the biaxial testing machine, a preload of 10 mN was applied in both axes to ensure straightening of the sample. Applying a quasi-static strain rate of $\dot{\varepsilon} = 0.1\%/s$, the sample was equibiaxially stretched until sample failure. All tests were video recorded, allowing first stretch measurements within the tracking area with respect to the reference state and second to check when tears appeared in the hook insertions. This information helps to better interpret the mechanical results during post-processing. Note, in order not to distort the results in the sense of the reference state, cf. Section 2.2.1, tissue samples were not preconditioned, as was done in [51], for example.

*2.2.3. Mechanical data analysis*

By performing stretch-controlled equibiaxial tension experiments, two forces ($f_1$ in the circumferential and $f_2$ in the longitudinal direction) were measured, see Fig. 4(a). Due to the microstructural conditions, the SW is mechanically inhomogeneous and anisotropic, which in turn might lead to shear deformation and thus to shear force. Consequently, all forces (two normal $f_{11}$, $f_{22}$ and two shear forces $f_{12}$, $f_{21}$) acting on the tissue samples (c) were unknown. In general, there are different strategies in the literature for determining these unknowns, cf. overview in [51]. However, we follow the procedure presented in [51], where homogeneous deformations within the central tracking area, see Fig. 4(b), and tissue incompressibility are assumed to quantify numerically in a post-processing step the stretches

$$\lambda_1 = \frac{\partial u_1}{\partial X_1} + 1, \ \lambda_2 = \frac{\partial u_2}{\partial X_2} + 1, \ \text{ and } \ \lambda_3 = \frac{1}{\lambda_1\lambda_2 - \gamma_1\gamma_2} \tag{1}$$

and in-plane shear

$$\gamma_1 = \frac{\partial u_1}{\partial X_2} \ \text{ and } \ \gamma_2 = \frac{\partial u_2}{\partial X_1}, \tag{2}$$

to be components of the deformation gradient $F_{ij} = \partial u_i/\partial X_j + \delta_{ij}$ with respect to the coordinate system given in Fig. 4. The deformation gradient at any arbitrary point within the tracking area is determined from the displacement of the markers by means of isoparametric interpolation [69]. Thereby, $u_i$, $X_i$, and $\delta_{ij}$ are the displacements, reference coordinates, and the well-known Kronecker delta, respectively.

Following Fig. 1(d), for each tissue sample (coloured in red), four additional samples (coloured in blue) were available, used to perform cross-sectional histological sections, which are necessary to determine sample-specific thickness ($T$). Sample-specific lengths in both directions ($L_1$, $L_2$) were measured from the reference state image. Having these measures and the forces acting on the tracked areas as illustrated in Fig. 4(c) at hand, the normal stresses

$$\sigma_{11} = \lambda_1 \frac{f_{11}}{L_2 T} + \gamma_1 \frac{f_{12}}{L_1 T} := \sigma_{\mathrm{circ}} \text{ and } \sigma_{22} = \lambda_2 \frac{f_{22}}{L_1 T} + \gamma_2 \frac{f_{21}}{L_2 T} := \sigma_{\mathrm{long}} \tag{3}$$

as well as shear stresses

$$\sigma_{12} = \lambda_2 \frac{f_{12}}{L_1 T} + \gamma_2 \frac{f_{11}}{L_2 T} = \lambda_1 \frac{f_{21}}{L_2 T} + \gamma_1 \frac{f_{22}}{L_1 T} = \sigma_{21} := \sigma_{\mathrm{shear}} \tag{4}$$

can be calculated in a straightforward manner.

After determining sample-specific stress-stretch relationships by simultaneous consideration of the reference state, see Section 2.2.1, the results of the samples were differently shifted based on the individual $\lambda_{\mathrm{pre}}$, see Fig. 2(b). Based on the huge variation of the stretch range, the results of the four samples within the same set of experiments were normalised in the following way: For each of the four tests, the domain of the stress-stretch relationship was mapped onto the unit interval, allowing the calculation of the mean and standard deviation. Afterwards, the average stress-stretch relationship was transformed back by mapping the unit interval to the interval [1, $\lambda_{\mathrm{max,mean}}$] by

$$g(\lambda) = (\lambda_{\mathrm{max,mean}} - 1)\lambda + 1 \text{ with } \lambda \in [0, 1], \tag{5}$$

whereby $\lambda_{\mathrm{max,mean}}$ defines the average stretch of the maximum stretches reached in the four individual tests. In this way, one stress-stretch relationship for each of the 21 cases was obtained.

### 2.3. Microstructural investigations

To study the wall's microstructure, i.e., the thicknesses of the various layers, the SM fibre distribution, and the composition of the muscular layer across the entire stomach, three stomachs were examined. Three right sides and one left side were used, while the left side was used to verify the symmetry of the SW. Every half of the stomach was subdivided into 5 × 5 rectangular samples ($n = 25$), equally distributed throughout the stomach half and fast-frozen within three hours of arrival at the laboratory, see also Remark 2.

Microstructural characterisation of the SW is based upon histological investigations. As previously described in detail by Morales-Orcajo et al. [51], these investigations primarily consist of three steps: Fast-freezing of the samples to avoid ice crystal formation and sample shrinkage, cutting thin sections in different planes, and staining these sections to contrast various constituents. Each of the 25 rectangular samples was cut into two equally sized sub-samples and denoted as IP for in-plane or CS for cross-sectional section. To determine the fibre distribution and the proportions of individual constituents, i.e., SM fibre, ECM, elastin, and fat, inside the muscular layer, 6 times 3 in-plane sections, featuring a thickness of 6 µm, uniformly distributed over the height of the muscular layer, were examined on the sub-samples IP. All samples were stained with Picro-Sirius red (staining of SM fibres and ECM). Additionally, samples of one stomach half were stained with Elastica van Gieson (staining of elastin) and Sudan III (staining of fat). To further determine the individual layer thicknesses, 2 cross-sections were created of all sub-sample CS. At both positions, samples were again stained with Picro-Sirius red, Elastica van Gieson, and Sudan III. For further analysis, the resulting sections, i.e., 800 Picro-Sirius red stained sections, 200 Elastica van Gieson stained sections, and 200 Sudan III stained sections, were digitalised and evaluated using the image analysis software ImageJ (FiJi project, NIH, USA).

To measure the layer thicknesses, a perpendicular line was drawn over the cross-section of each digitised image, and the distance between the intersections of the layers with the line sections determined the thickness of each layer. Furthermore, orientations of the SM fibre bundles were measured across the stomach. Therefore, by analysing the digitised images of the in-plane sections with respect to the organ axes, fibre bundle orientations were assessed by evaluating the structure tensor of every pixel within the region of interest [61]. Frequently used in image processing the structure tensor contains the information about the predominant direction in the local neighbourhood of a pixel. Finally, the composition of the muscular layer was quantified by means of the amount of SM fibres, ECM, and fat. The default threshold over the green channel was applied to enhance the ECM, i.e., red pixels, over the SM fibre bundles in the Picro-Sirius red stained sections, allowing the quantification of the number of pixels of ECM with respect to the total. The same threshold was applied to the Sudan III stained sections, enhancing fat, i.e., red pixels, over the white background. Furthermore, the amount of elastin within the ECM was measured in Elastica van Gieson stained sections. Detailed information related to the staining protocols can be found in Appendix B.

**Remark 2.** [Idealised stomach geometry] Due to the natural anatomical variability between animals, it was not possible to systematically match the 25 sample locations between specimens, i.e., the four stomach halves. Thus, for analytic and visualisation purposes, the four specimens were mapped into an idealised geometry of the stomach. In the following, this idealised geometry is used to illustrate the distribution of several parameters across the organ.

### 2.4. Morphological and micromechanical load transfer mechanisms in the stomach wall

In view of the complex morphology and microstructure of the SW, it is readily apparent that during mechanical loading, there is a complex interplay between the individual layers and the constituents therein. E.g. during stomach loading the intragastric pressure remains relatively low while in-wall deformations increase significantly. Consequently, this effect is only due to the morphological and microstructural structure of the SW and their specific load-transfer mechanisms, to be so far unexplored.

To gain insight into these mechanisms, samples from the fundus were equibiaxially loaded up to specific stretch levels of $\lambda = 1.2/1.35/1.5/1.8$ and then fast-frozen in their deformed state. In more detail, after biaxial stretching of the tissue samples to the aimed stretch level, thin metal pins attached to a small rigid frame were pressed into the tissue around the region of interest so that it could no longer move mechanically. In this situation, the tissue with the frame was fast-frozen. Microstructural changes were assessed by comparing histological cross-sections of unloaded sample-surrounding-tissue with histological cross-sections of loaded samples. The average thickness of the unloaded sample-surrounding-tissue ($T_{\mathrm{unloaded}}$) was measured in four cross-sections, one per side, and the average thickness of the loaded sample ($T_{\mathrm{loaded}}$) was determined in four cross-sections within the sample, mirroring the unloaded cross-sections. Then, the thinning response was calculated as

$$\mathcal{T} = \left(1 - \frac{T_{\mathrm{loaded}}}{T_{\mathrm{unloaded}}}\right) \times 100. \tag{6}$$

A total of sixteen samples were tested, four samples for each stretch level.

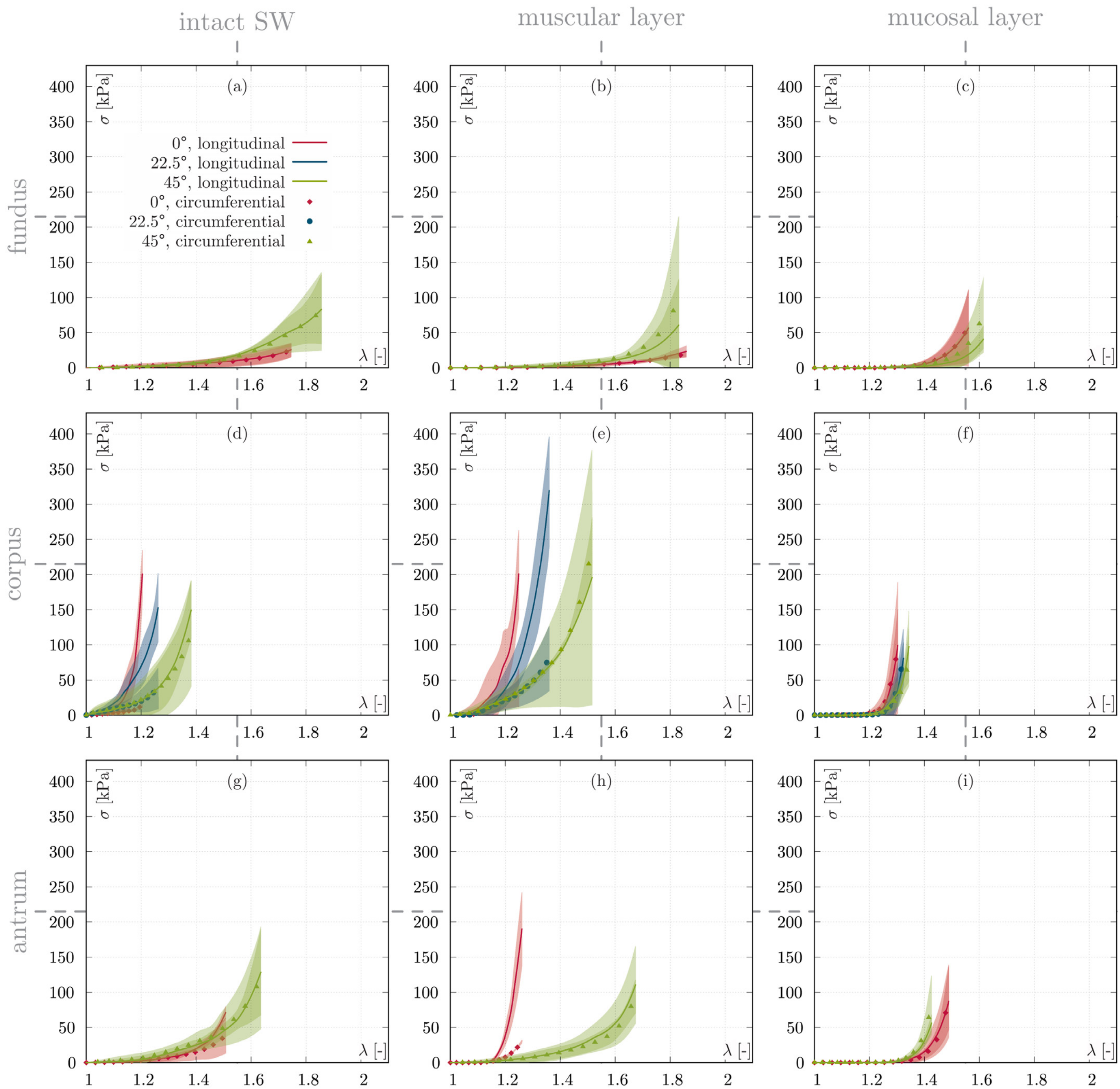


**Fig. 5.** Location-, layer-, and orientation-dependent stress-stretch behaviour of the SW. Solid curves and signs characterise mean longitudinal and circumferential values, respectively. Shaded areas depict standard deviations, each calculated from four single tests.

## 3. Results

### 3.1. Mechanical properties of the stomach

Following Section 2.2, samples for the mechanical experiments were sorted by region, orientation, and layer. In the first step, orientation-dependent equibiaxial experiments on tissue samples of the entire SW, the muscular layer, and the mucosal layer are realised for each of the three regions. The mechanical responses in the form of stress-stretch relationships are presented in Fig. 5. Herein, solid curves and signs characterise mean longitudinal and circumferential values (normalised by the stretch, cf. Section 2.2.3), respectively.

When analysing the stress-stretch curves, different characteristics can be identified: By comparing region-dependent characteristics of the intact SW, a strong orientation dependency of the corpus was detected. From analyses of the stress-stretch curves, several patterns were observed: First, the intact wall in the corpus exhibits strong orientation dependency. Samples oriented parallel to the greater curvature, i.e., 0°, show high anisotropy (solid line (longitudinal) and signs (circumferential) of the same biaxial experiments differ) with higher stresses, cf. (d). While the degree of anisotropy is reduced in samples oriented 22.5°, cf. (d), it disappears in case of 45° sample orientation (solid line (longitudinal) and signs (circumferential) of the same biaxial experiment agree). In direct comparison, this characteristic can also be seen in the

**Table 1**
Average shear behaviour of all samples tested ($n = 21$). Values were computed as the means of the absolute values at the maximum stretch from four single tests.

| Region | Layer | Orientation | Shear deformation | | Shear stress | Stress ratio | |
|---|---|---|---|---|---|---|---|
| | | | $\gamma_{long}$ | $\gamma_{circ}$ | $\sigma_{shear}$ | $\sigma_{shear}/\sigma_{long}$ | $\sigma_{shear}/\sigma_{circ}$ |
| | | [°] | [-] | [-] | [kPa] | [%] | [%] |
| fundus | intact SW | 0 | 0.13 | 0.06 | 1.12 | 4.4 | 4.5 |
| | | 45 | 0.11 | 0.07 | 2.24 | 2.7 | 2.8 |
| | muscular layer | 0 | 0.23 | 0.11 | 0.98 | 4.2 | 4.9 |
| | | 45 | 0.09 | 0.06 | 1.46 | 2.4 | 1.5 |
| | mucosal layer | 0 | 0.03 | 0.05 | 1.23 | 2.1 | 2.0 |
| | | 45 | 0.03 | 0.07 | 0.38 | 0.9 | 0.5 |
| corpus | intact SW | 0 | 0.05 | 0.06 | 5.82 | 3.1 | 39.5 |
| | | 22.5 | 0.02 | 0.24 | 16.98 | 11.1 | 44.4 |
| | | 45 | 0.21 | 0.34 | 30.43 | 19.9 | 25.7 |
| | muscular layer | 0 | 0.07 | 0.08 | 8.37 | 4.1 | 21.5 |
| | | 22.5 | 0.17 | 0.19 | 25.27 | 8.0 | 31.5 |
| | | 45 | 0.46 | 0.38 | 70.71 | 33.8 | 23.3 |
| | mucosal layer | 0 | 0.04 | 0.03 | 1.64 | 1.6 | 1.7 |
| | | 22.5 | 0.02 | 0.04 | 1.61 | 1.9 | 1.9 |
| | | 45 | 0.09 | 0.09 | 5.31 | 5.4 | 6.4 |
| antrum | intact SW | 0 | 0.13 | 0.08 | 2.82 | 2.5 | 3.3 |
| | | 45 | 0.10 | 0.06 | 4.92 | 3.8 | 4.1 |
| | muscular layer | 0 | 0.09 | 0.09 | 9.21 | 4.5 | 12.8 |
| | | 45 | 0.16 | 0.1 | 8.09 | 7.2 | 8.6 |
| | mucosal layer | 0 | 0.06 | 0.03 | 2.29 | 2.6 | 2.4 |
| | | 45 | 0.03 | 0.03 | 0.82 | 1.4 | 1.0 |

muscle layer of the corpus. Accordingly, samples oriented parallel to the greater curvature feature the highest degree of anisotropy, diminishing when samples are rotated, see (e). In contrast, the mucosal layer of the same region exhibits the same response in all orientations. Therefore, the material behaves independently of its orientation, isotropic. Further, a large initial stretch of about $\lambda_{pre} = 1.2$ with zero stress, followed by a pronounced change of the slope with almost no differences between the orientations, cf. (f), was observed for the mucosal layer of the corpus. Therefore, the intact SW properties and those of the muscular layer of the corpus show anisotropic behaviour, whereas the mucosal layer exhibits rather isotropic characteristics. Further, by comparing the failure stretches of intact SW, muscular layer, and mucosal layer, a sequence of order becomes apparent: The lowest failure stretch can be seen for the 0° samples followed by the 22.5° and 45° samples.

In the antrum, intact SW features the same response independently of sample orientation, cf. (g). The samples from the two orientations (longitudinal vs. circumferential) differ in their failure stretch at 1.51 and 1.64 for 0° and 45° oriented samples, respectively. The muscular layer presents a fibre dependent behaviour as function of the sample orientation, cp. (h). Thus, while a significant anisotropic behaviour can be recognised for 0° oriented samples, the stress-stretch response for 45° oriented samples features isotropic behaviour. As such, the mucosal layer of the antrum behaves, with respect to maximum stresses, similarly to the mucosal layer of the corpus. However, the failure stretches are clearly different.

In the fundus, the mechanical behaviour of the intact SW and muscular layer is similar, reaching higher stretches and lower stresses compared to the other regions. The isotropic stress-stretch characteristics are recognisable, independent of sample orientation, cf. (a) and (b). In contrast to all other regions, this behaviour can be bisected; a first nearly linear stress-stretch relation (almost up to a stretch of $\lambda = 1.6$) is followed by a nonlinear curve. Further, the mucosal layer of the fundus is more stretchable and reaches lower stresses than the mucosal layers of other regions, cf. (c). Thus, within the fundus, all layers exhibit isotropic behaviour.

In the direct comparison of the three regions, the highest stress is observed in the corpus. The fundus and antrum exhibit similar maximum tension stresses, although these tend to be lower in the fundus, especially for experiments on samples of intact SW and the muscular layer. Finally, when focusing on the pre-stretches $\lambda_{pre}$ for intact SW, muscular layer, and mucosal layer, increasing averaged pre-stretches of $\lambda_{pre} = 1.10$, $\lambda_{pre} = 1.14$, and $\lambda_{pre} = 1.26$ are observed, respectively.

Additionally, for all tested samples, shear stresses were determined by computing the deformation gradient from the nine-dot grid, as described in Section 2.2.3. In Table 1 the shear response is summarised by computing absolute values at the maximum stretch. The intact wall and the muscular layer of the corpus exhibit a strong relationship between shear stress and sample orientation. Shear stresses ($\sigma_{shear}$) and shear deformations ($\gamma_{circ}$ and $\gamma_{long}$) increase as the sample is rotated from 0° to 45°. The mucosal layer of the corpus exhibits low shear stresses at all orientations, i.e., is independent of sample orientation. As previously stated, the intact wall and muscular layer of the corpus exhibit anisotropic behaviour with strong dependency on sample orientation with respect to the testing axes, whereas the mucosal layer behaves in an isotropic fashion. In the antrum, the intact wall, and the muscular layer exhibit higher stresses than the mucosal layer, which does not change with orientation. Overall, the fundus presents low shear stress and deformation at all layers and orientations in the order of magnitude of the shear values of the mucosa.

### *3.2. Stomach microstructure*

#### *3.2.1. Cross-sectional wall profile of the stomach*

Compared to other hollow organs, e.g., the urinary bladder [14,51], the cross-sectional wall profile of the stomach is characterised by tremendous heterogeneity, see Fig. 6. The intact SW has an average thickness of 6.6 ± 1.4 mm, although this value can be misleading since there exist large differences among distinct regions. For example, the fundus shows a relatively constant thickness of 6.1 ± 1.4 mm, while the SW in the antrum is the thickest and shows a relatively constant thickness of 7.93 ± 0.25 mm (c). In contrast, the fundus and corpus possess thinner SW and

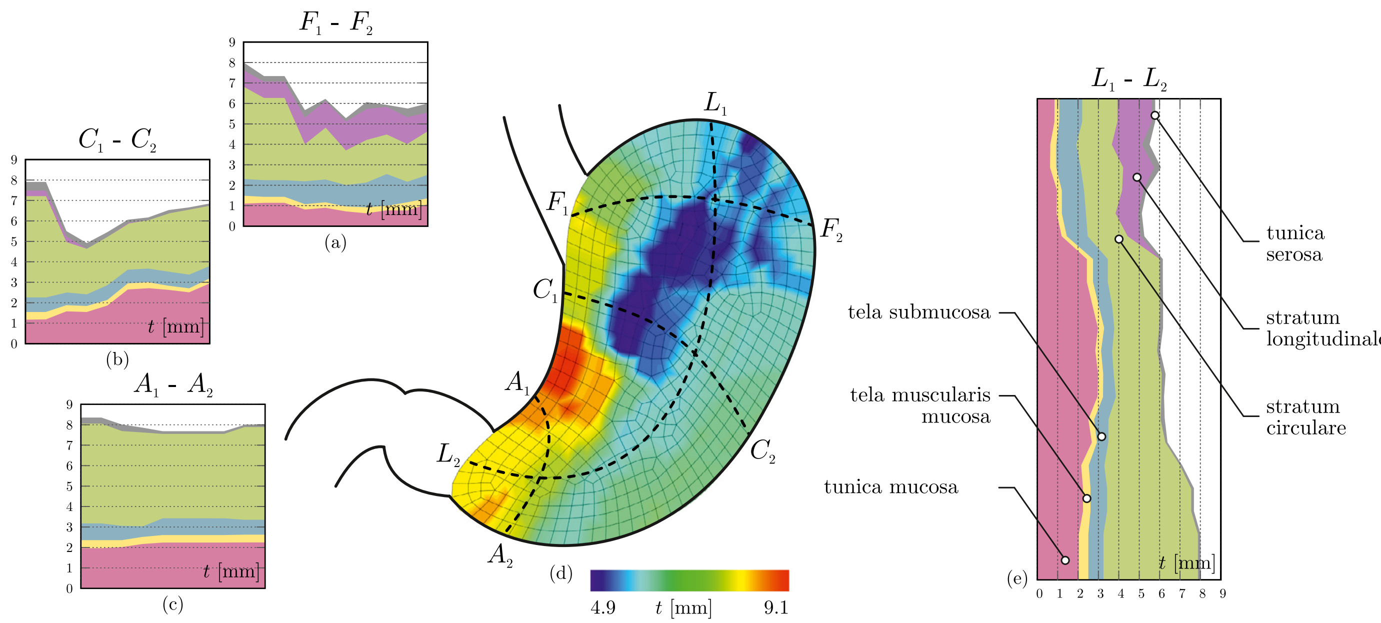


**Fig. 6.** Stomach wall thickness across the entire organ. Thickness of the intact wall mapped on the idealised stomach shape sketch (centre). Three circumferential (left) and one longitudinal profile section (right) illustrate the thickness evolution of each layer across each region. Note, all values shown are the mean of four specimens ($n = 4$). For layer-specific thicknesses, see Fig. 11 in Appendix A.

much larger variations in thickness, ranging from 8 to 5 mm (mean 6.36 ± 0.84 mm, cf. (a)) and from 8 to 5 mm (mean 6.39 ± 0.94 mm, cf. (b)), respectively. This increase in SW thickness from the fundus to the antrum is shown following a virtual line $L_1$ to $L_2$, cf. (e), along the stomach wall. As SW thickness decreases from the lesser to the greater curvature of the fundus (a), it exhibits its minimum value between both curvatures in the corpus (b), remaining nearly constant in the antrum (c). The cardia is located around the oesophageal sphincter. Together with the antrum, these comprise the thickest regions of the stomach. The tunica mucosa consists of the epithelium, the lamina propria, and the gastric pits. The corpus possesses the thickest mucosa, 2.2 ± 0.9 mm, followed by the antrum with 2.1 ± 0.5 mm, whereas the fundus has a thinner tunica mucosa featuring 0.9 ± 0.4 mm. The tela muscularis mucosa, part of the mucosal layer, is a clearly distinguishable slender layer consisting of thin smooth muscle fibres densely packed into an ECM that pulls the mucosa into folds to increase the surface area of digestion and absorption [54]. It is the most consistent layer of the SW, featuring a uniform thickness of 0.3 ± 0.1 mm across the entire organ, becoming slightly thicker in the antrum. The tela submucosa, located between the tela muscularis mucosa and the muscular layer, is a rich network of connective tissue embedded with blood and lymphatic vessels, submucosal glands and nerves, i.e., mechanoreceptors, and connecting the tunica mucosa and muscular layer [47,54]. In the corpus the tela submucosa features a small thickness of about 0.6 mm and consists of dense ECM with almost no fat, see also Fig. 7(b).

However, in the rest of the stomach, especially the fundus, the submucosal layer contains massive clusters of fat cells embedded in the ECM, increasing the thickness to 1.1 mm in the fundus and 0.8 mm in the antrum. The tela submucosa fills the gaps formed between the folded mucosa and the straight muscular layer, see also Fig. 7(a). Beyond the submucosal layer lies the muscular layer, a thick layer of smooth muscle fibre bundles arranged in different orientations and responsible for the active behaviour of the SW. The circular muscle layer (stratum circulare) is present from the fundus to the antrum (d), exhibiting its highest thickness (up to 5.5 mm in the lesser curvature) in the antrum (c). Interestingly, the longitudinal muscle layer (stratum longitudinale) is especially pronounced in the fundus, see (a) and (e). In contrast, the longitudinal muscle layer is very thin in the corpus (b) and almost nonexistent in the antrum (c). Thus, only the fundus is characterised by a complex arrangement of two wavy muscular layers of similar size, running cross-oriented to each other with a total thickness of 3.5 ± 1.5 mm, see Fig. 7(a). Finally, the outermost layer of the stomach wall is the serosal layer, a very thin collagen layer of 0.2 ± 0.2 mm spanning the entire stomach and serving as a structural outer coat.

In summary, the photorealistic reconstructions in Fig. 7 clearly show how differently the various layers are distributed across the three regions. Above all, the strong waviness of the muscular layers in the fundus (a) is noticeable. Both layers (stratum circulare and stratum longitudinale) run nearly perpendicular to each other. From the mechanical perspective, interweaving of both layers is of high interest, see in-plane sections in Fig. 7, especially IP4 and IP5. While the fundus is very inhomogeneous, the other regions, corpus (b) and antrum (c), exhibit a rather compact structure. In the antrum, the relatively thick muscle layer is particularly noticeable, whereas in the corpus, the submucosa is very small.

### 3.2.2. Smooth muscle fibre bundle orientation

An important factor determining the contraction directions within the SW is the orientation of the SM fibre bundles. In Fig. 8, orientations of the SM fibre bundles throughout the muscular layer (stack of 6 in-plane sections, see also enlargement of Fig. 7(a)) across the entire stomach are illustrated. For a more detailed description of the underlying concept, see Remark 3. At first glance, wide dispersion is observed in the fundus compared to the corpus and antrum. The corpus and antrum exhibit highly oriented fibre bundles perpendicular to the greater curvature, i.e., circumferential orientation, constant in thickness. However, the fundus presents a less uniform structure with at least two different orientations and high dispersions. In the region of the lesser curvature, an oblique-oriented layer is distinguished in the outer sections with respect to the circumferential inner ones. In the fundus, two cross orientations are observed. The inner sections (black coloured orientations) with smaller standard deviation are somehow circumferentially oriented, but in the outer part (light grey

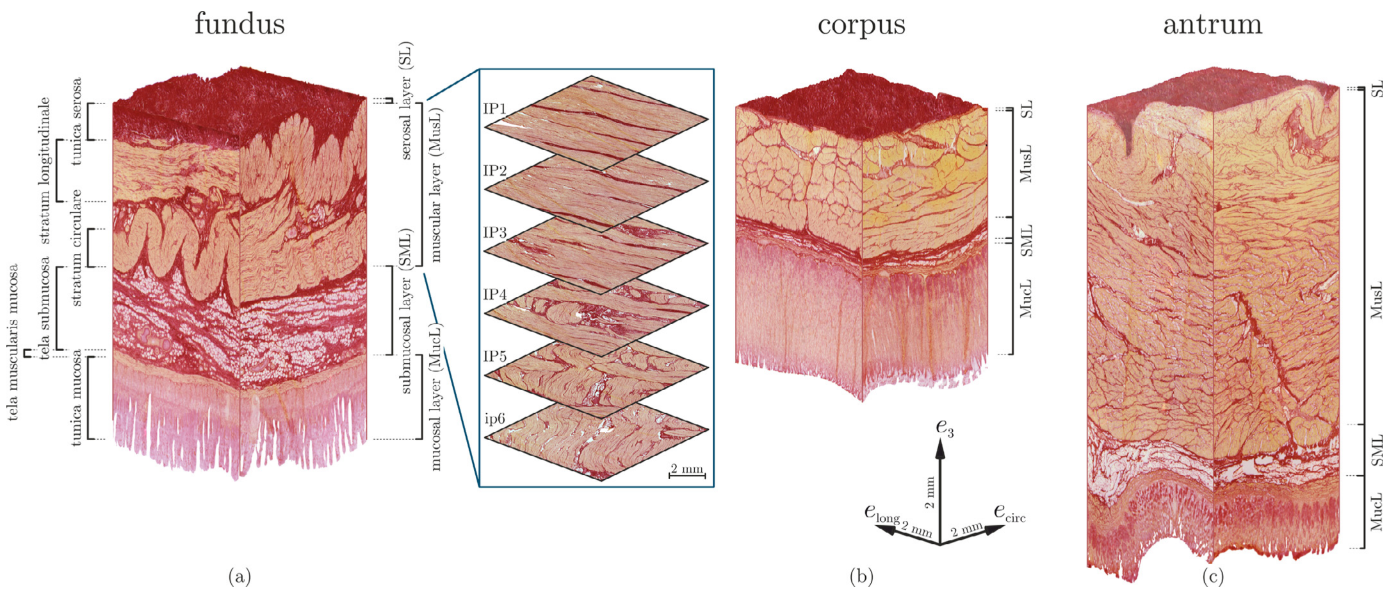


**Fig. 7.** Photorealistic three-dimensional reconstruction of the stomach wall in the (a) fundus, (b) corpus, and (c) antrum based on histological cross-sections of perpendicular planes. Note, each arrow length of the coordinate system corresponds to 2 mm. Further, a z-stack of 6 in-plane sections of the fundus is represented.

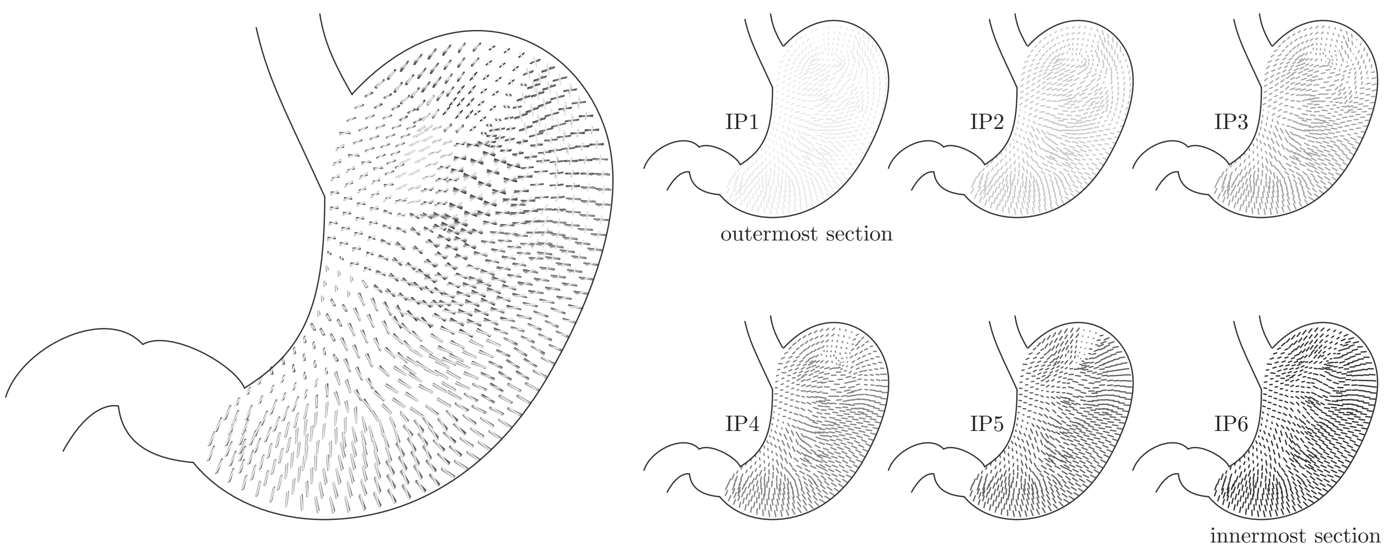


**Fig. 8.** Muscle fibre bundle orientation in the muscular layer from the outermost (IP1) to the innermost (IP6), cf. Fig. 7 (a), across the entire organ. Orientations are plotted as vector fields (to be the eigenvectors of the mean structure tensor), and each vector indicates the orientation with the vector length (to be the corresponding eigenvalue of the mean structure tensor) describing the degree of orientation. Consequently, a long vector indicates a strong orientation, and a short vector indicates a highly dispersed orientation. Orientation changes in the transmural direction are plotted in different colors from light grey (outermost) to black (innermost).

orientations), there is no recognisable pattern. Such variation may be explained by the fundus' complex microstructure as illustrated in Fig. 7(a). Apparently, two wavy layers run cross-oriented and partly interwoven in the intersection between the layers. These two muscular sublayers vary in thickness and waviness as a function of their location, losing their waviness and merging in a unique layer as they approach the distal corpus. The fundus striae also reveal an intrinsic discontinuity of the orientation pattern in the outer layer. Viewing the stomach from the outside, clearly distinguishable abrupt changes in the fundus striae orientation are visible, see Fig. 1(c). Furthermore, extension of the regions varies significantly between specimens. For example, we observed that the extension of the fundus gastric rugae can vary from 15% to 45% of the total length. However, all these features together make mismatching the orientation easy among samples from the same location and deepness, reflected by the large deviations we obtained.

**Remark 3.** [Average preferred fibre orientation] The mean structure tensor of all stomach samples provides a direct access to the average preferred fibre orientation. Herein, the eigenvalues and eigenvectors of the tensor indicate the degree of anisotropy and the corresponding preferred orientation of the SM fibre bundles.

### 3.2.3. Composition of the muscular layer

The composition of the muscular layer, independent of the fibre orientation, is more or less similar across all regions, see Table 2. In general, the muscular layer is composed of 80.9% SMCs, embedded in 17.9% ECM, and 1.1% small fat cell clusters, although there are small variations between regions. In all regions, there is more than double the fat content in the outer sections compared to the inner sections. In the cross-sections, accumulation of fat cell clusters is observed in the outer half of the muscular layer, cf. Fig. 7(b) and (c).

**Table 2**
Region-specific composition of the muscular layer, determined from the outermost section (IP1) adjacent to the serosa layer to the innermost section (IP6) next to the submucosal layer, cp. Fig. 7(a).

| | regions | | | | | | | | | total | | |
|---|---|---|---|---|---|---|---|---|---|---|---|---|
| | fundus | | | corpus | | | antrum | | | | | |
| IP | SMC [%] | ECM [%] | fat [%] | SMC [%] | ECM [%] | fat [%] | SMC [%] | ECM [%] | fat [%] | SMC [%] | ECM [%] | fat [%] |
| 1 | 75.2 | 23.7 | 0.9 | 80.4 | 18.0 | 1.4 | 80.3 | 17.8 | 2.0 | 78.7 | 19.8 | 1.3 |
| 2 | 79.6 | 18.6 | 1.4 | 81.7 | 16.4 | 2.0 | 81.3 | 16.5 | 2.4 | 81.0 | 17.1 | 1.8 |
| 3 | 79.4 | 19.6 | 0.9 | 81.8 | 16.5 | 1.7 | 82.6 | 15.9 | 1.4 | 81.3 | 17.3 | 1.3 |
| 4 | 79.2 | 20.1 | 0.6 | 82.2 | 16.6 | 1.1 | 80.7 | 18.3 | 0.9 | 81.0 | 18.0 | 0.9 |
| 5 | 80.2 | 19.4 | 0.3 | 82.5 | 16.9 | 0.7 | 82.9 | 16.4 | 0.7 | 81.8 | 17.6 | 0.6 |
| 6 | 79.7 | 19.8 | 0.3 | 82.8 | 16.2 | 1.0 | 81.9 | 17.2 | 0.8 | 81.7 | 17.6 | 0.7 |
| **mean ± s.d.** | **78.9 ± 6.9** | **20.2 ± 6.6** | **0.7 ± 1.0** | **81.9 ± 5.7** | **16.8 ± 5.4** | **1.3 ± 1.3** | **81.6 ± 7.4** | **17.0 ± 7.0** | **1.3 ± 1.4** | **80.9 ± 6.4** | **17.9 ± 6.1** | **1.1 ± 1.2** |

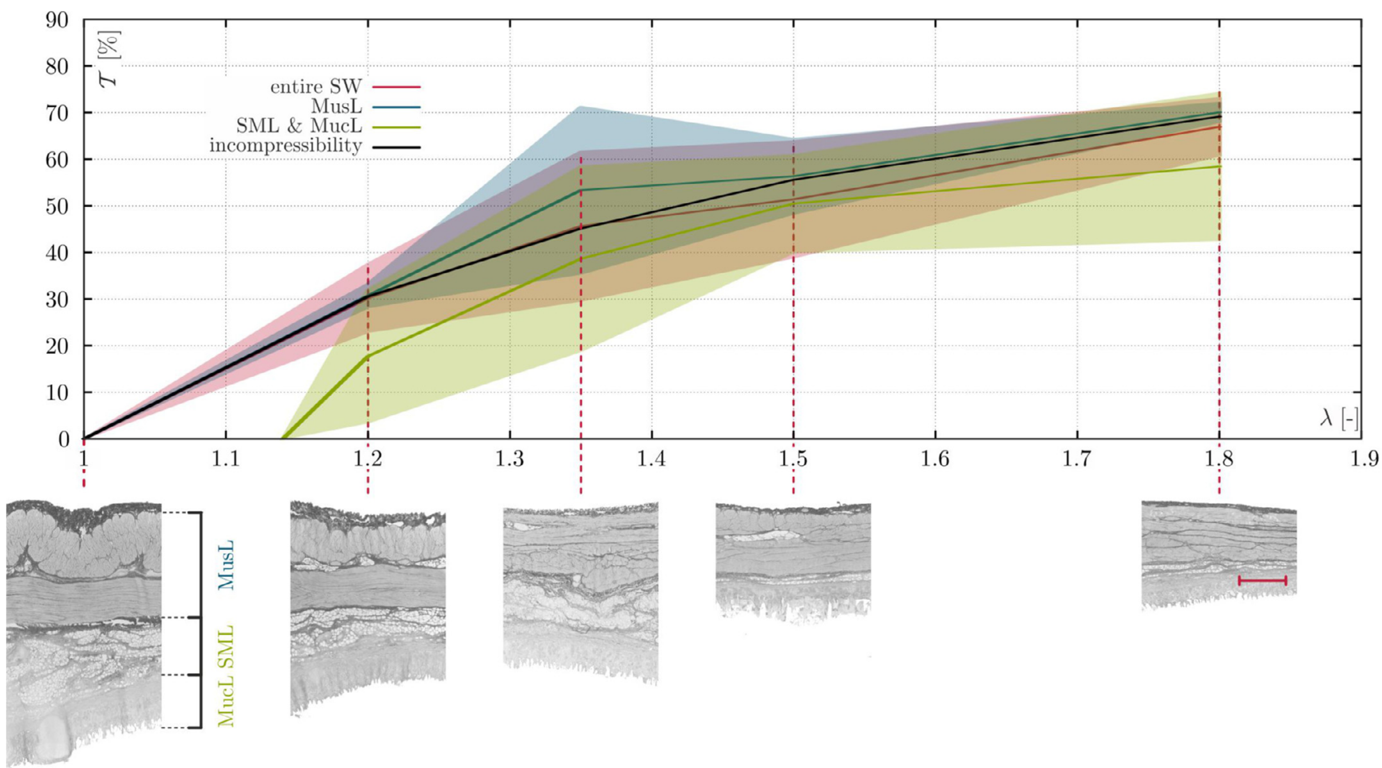


**Fig. 9.** Thinning behaviour of the fundus' main layers: Layer-specific thinning characteristics and histological images of the SW at discrete stretch levels $\lambda$ = 1:0/1:2/1:35/1:5/1:8. Note, abbreviation for the layers were taken from Fig. 7. Scale bar: 1 mm.

As mentioned earlier, the ECM consists of elastin and collagen fibres, and the present study demonstrates that the elastin content is very low in the muscular layer. Scattered elastin fibres were found running parallel to the smooth muscle fibre bundles, accounting for less than 0.5% of the total composition.

### *3.3. Microstructural changes under loading conditions*

One essential issue with respect to tissue engineering is the question of how loads are transferred within the SW. The wavy structure of the muscular and mucosal layers, see e.g., Fig. 7, seem to play a central role in this process. To shed light on this question, the thinning response of fundus cross-sections under increasing deformation was analysed, see Fig. 9.

The muscular layer shows a nearly incompressible response at all stretch levels. On the other hand, the mucosal layer is located far below the incompressibility behaviour, particularly at the beginning. This is explained by the reference state of the samples. At $\lambda = 1.0$, the muscular layer is straight, but the mucosal layer is folded, see Fig. 2. During the first 14% of the deformation, the mucosa is unfolding, only slightly bearing the load. Once the mucosa is straight, it starts to deform, i.e., becoming thinner. Meanwhile, the intact wall shows the combined response of the incompressible muscular layer and the folded mucosal layer, located between both curves, since the total thickness is the sum of both layers and the submucosal layer.

## 4. Discussion

The present study demonstrates that the microstructure of the SW is highly heterogeneous across the organ, impacting its mechanical properties. To the best of the authors' knowledge, this is the first study examining (i) the location-orientation and layer-specific mechanical properties of the SW through biaxial testing, (ii) the microstructure of the SW in terms of layer thicknesses, composition, and muscle fibre bundle orientation, and (iii) load transfer mechanisms that occur in the SW and influence the relationship of mechanical and structural variation across the stomach.

### 4.1. Stomach wall mechanical properties

One essential goal of this study was to elucidate the mechanical characterisation of the SW. The morphology of the layers (e.g. the waviness of the mucosal and muscular layers) and their microstructure (e.g. the fibre orientation) significantly influences mechanical results. Therefore, the mechanical results shown in Fig. 5 have been attained with consideration of both, the morphology and the microstructure to be able to make a conclusion about load transfer mechanisms, which is essential for tissue engineering strategies.

In a variety of studies, biological tissue is preconditioned using varying numbers of loading and unloading cycles to achieve a so-called 'equilibrium state' in which the curves are repeatable and stable to determine the mechanical properties of the tissues. Although this step is widely used in soft biological tissue testing, there is no standardised protocol [51], with the exception of some general recommendations, such as that the maximum stretch level and strain rate should match the intended test. However, with respect to stomach biological testing, the number of preconditioning cycles varies between zero [21,62,63] over 2 [33,75,76] to a maximum of 7 cycles [6]. In all these studies, it remains questionable whether the tissue truly is at an equilibrium state and what that means with respect to the stomach's physiology. The latter point is of great interest, since under physiological conditions, i.e., in vivo, preconditioning effects cannot be observed. To determine the most realistic material properties of the stomach under normal physiological conditions, the tissue was not preconditioned in the present study.

A fundamental issue with sampling soft, biological tissue is to what extent tissue handling influences the mechanical tissue properties before the actual sampling. Further, when sampling individual layers, which in some cases exhibit waviness that is not negligible in their reference state, to be the in vivo situation, see Fig. 2, precise mechanical sampling under consideration of the reference state is indispensable. This waviness is directly correlated with the stomach function, as it influences the mechanical characteristics of the muscular and mucosal layer. While the muscular layer is responsible for the stomach motility, the mucosal layer, apart from regulating the chemical activity, restrains the stomach deformation at high pressure. These two layers deform independently thanks to the loose submucosal layer between them [42,55]. All these structural features need to be considered when mechanical properties are examined, and this procedure is a key step for correctly comparing the mechanical contribution of isolated layers to the compound response of the intact multi-layered structure. Thus, in this study, sampling history was tracked throughout the whole process, from sample excision to final mechanical biaxial testing, cf. Section 2.2.1. This deformation, denoted as 'pre-stretch' $\lambda_{\text{pre}}$ within the present study, was identified in terms of mean values of all samples and over all regions (fundus, corpus, antrum) as $\lambda_{\text{pre}} = 1.10$, $\lambda_{\text{pre}} = 1.14$, and $\lambda_{\text{pre}} = 1.26$ for the intact SW, muscular layer, and mucosal layer, respectively. Basically, all layers exhibited a pre-stretch, which was particularly high in the mucosal layer, since this layer has the strongest waviness. By considering the pre-stretches, as done in this study, the stress responses of the individual layers as well as the entire SW samples are shifted based on their individually determined pre-stretches, i.e., $\lambda = \lambda_{\text{pre}}$, see also Fig. 2(b). This shift has a clear influence on the tissue load transfer mechanism, cf. Fig. 9: During tensile loading of the SW, first the muscular layer is bearing loads, and the folds of the mucosal layer are straightened. As shown in Fig. 5, for low stretches the stress response of the mucosal layer remains zero. This however, implies that elastic deformations are negligible. This state represents a stress-free configuration of the mucosa and muscle layer with a significantly reduced waviness. For higher stretches, elastic deformations become more relevant and stresses increase. When the mucosal layer reaches its pre-stretch, it contributes to the load transfer. The total deformation of the tissue layer is split into two components, namely the pre-stretch and the elastic component, which describes the actual mechanical response of the constituents within the tissue layer. So far, this pre-stretch effect, which is influenced by handling and fold straightening, has not been considered in studies dealing with SW characterisation [6,21,33,62,63,75,76]. When focusing only on the influence of fold straightening, only two studies can be considered, as they performed layer-specific experiments on SW tissues [33,76]. In both studies, the authors applied uniaxial tension experiments on the intact SW, the muscular layer, and the mucosal layer. For all layers, independent of the region, the stress-stretch relationship starts at $\lambda = 1$, indicating that the pre-stretch effect was not considered.

Considering the aforementioned effects, within this study, equibiaxial tension experiments were performed to identify the SW's region- and orientation-dependent, as well as layer-specific, mechanical characteristics. Results are summarised in Fig. 5. Overall, independent of the region and tested layers, the SW is characterised by clearly nonlinear material behaviour. The curves follow clear exponential courses, especially in the corpus and antrum. While the fundus did not exert a significant influence on tissue orientations in the tissue properties, in the corpus, an increase of tissue orientation angle led to a decrease in stiffness and an increase in isotropy and failure stretch. These results are in good agreement with the microstructural results in Section 3.2. Thus, the smooth muscle fibre bundles in the corpus are oriented substantially in the circumferential direction, see Fig. 8. Therefore, the 0° sample has the strongest anisotropy (the fibres are aligned in $\boldsymbol{e}_2$-direction, cf. Fig. 4, and consequently parallel to one axis of the testing machine), leading to increased stiffness and lower failure stretches. If the sample is now rotated by 45°, this yields a reduction in the degree of anisotropy. This in turn leads to a reduction in stiffness, while the failure stretches increase. It is especially surprising that for 0° samples, in which the fibres are aligned in the circumferential direction, the maximum stresses occur in the longitudinal direction, see Fig. 5(d), red line and (e), red signs, and not in the circumferential direction, as would be expected with classical fibre composites. However, the same observations were seen in the antrum, see (g) and (h), also featuring a fibre orientation in the circumferential direction, but the effect was not as pronounced as in the corpus. Even if this phenomenon seems to be counterintuitive, it may be explained by the stomach's functional side.

When the stomach is filled with food, it primarily experiences a circumferential expansion. This expansion must be able to be react without stress being highly increased in the circumferential direction; otherwise, failure of the SW would occur. This exact phenomenon of high stretches in response to simultaneous low stresses can be recognised here. Having the microstructure in mind, this means that for the same stress, the SW is more stretchable parallel to fibre direction than perpendicular to the fibres. As the fibres are embedded within the ECM, it can be assumed that the ECM bears the large stretches. This is in good agreement with the relatively high content of approximately 20% ECM inside the muscular layer, cf. Table 2.

While the aforementioned anisotropy effects take place in the muscular layer and in the intact SW, independent of the region, the mucosal layer is characterised by isotropic stress-stretch responses, see (c), (f), and (i), respectively.

Previous studies of the mechanical properties of the stomach show similar trends, such as isotropic mechanical characteristics of the fundus [6], stiffer mechanical behaviour in longitudinal compared to circumferential directions [33,75,76], and stiffer characteristics in the corpus than in the fundus [6,75,76]. However, comparisons of concrete stress and stretch values are difficult to perform, since all experiments were conducted under different testing conditions. Thereby, essential differences represent variations in deformation states, preconditioning procedures, or deformation rates.

It remains common practice in planar soft tissue characterisation to assume negligible shear stresses, as this is assumed to be very small compared to the principal stresses [e.g. 6, 52, 68]. However, based on the challenge of quantifying shear stress during biaxial testing, the error of this assumption was unknown. Recent biaxial tests accounting for shear stress have reported shear stress to be 1 to 2 orders of magnitudes lower than the principal stresses for myocardium [69] and urinary bladder wall tissues [51]. Within the present study, shear stresses were estimated through the assumption of planar homogeneous deformation within the central tracking area, cp. Fig. 4(b). Thereby, the use of markers was necessary to perform stretch-control tests. Following Table 1, with respect to dependence on the tissue orientation, the region, and the layer, the ratio of normal to shear stress was quantified to be between 2.25 and 200 times that for stretches up to 1.86. In doing so, the highest shear stresses are generally measured in the intact SW and muscular layer. Hereby, the corpus stands out as having the highest shear stresses measured, featuring a ratio of normal to shear stress of only 2.25.

To the best of the authors' knowledge, this is the first time that shear stress has been estimated for SW tissue. Aydin et al. [6] also performed biaxial tension experiments on SW tissue. However, the authors stated that the shear deformation components were typically two orders of magnitude smaller than the axial ones, and thus, negligible. Consequently, one primary finding of the present study is that in-plane shear stresses definitely exist in biaxially tested porcine SW. Basically, these shear stresses can be reduced to a minimum by effective preparation of the specimens and when the muscle fibre bundles are oriented along the axis of the testing machine, i.e., 0° oriented samples.

### 4.2. Stomach wall microstructure

Following Fig. 6, the intact SW thickness is clearly higher in the antrum than in the fundus and corpus. Among all three regions, the muscular layer is thickest in the antrum. The mucosal layer is thinnest in the fundus and becomes thicker in the greater curvature of the corpus. These findings are in good agreement with measurements by [76], who also measured the thickness of the SW and its layers. However, while Zhao et al. [76] only measured the intact SW, the muscular layer, as well as a combination of the mucosal layer and the tela submucosa, within the present study, additional finer sub-layers, such as the tela muscularis mucosa, and tela submucosa, were measured independently, see Fig. 6. The tela muscularis mucosa is a continuous thin band clearly visible that thickens as it approaches the pylorus, which was also reported by Keet [34]. The tela submucosa is located between the very thin tela muscularis mucosa and the significantly thicker muscular layer, featuring the highest thickness in the fundus and similar thickness between the corpus and antrum. It is rich in mast cells, macrophages, lymphocytes, eosinophilic leukocytes, and plasma cells, embedded by arteries, veins, lymphatic vessels, and nerve plexuses [34,47]. This loose connective tissue fills the space between the gastric rugae and the muscular layer [34,42,55] and is particularly prominent in the fundus, cf. Figs. 1(d) and 7. The muscular layer is located beyond the submucosa. In the fundus, two wavy cross-oriented layers merge into one muscular layer, see Fig. 7. The thickness of the muscular layer increases in the longitudinal direction, reaching a maximum in the antral pylorus end [49,76], cf. Fig. 6. Finally, the serosal layer builds the outer surface of the stomach. Following Fig. 6, the serosal layer is the thinnest layer, consisting of loose connective tissue closely attached to the muscular layer, except at the greater and lesser curvatures, where the serosal layer merges with the greater and lesser omentum, respectively [34].

Even if the orientation of the smooth muscle fibre bundle inside the muscular layer is one of the most important issues from the mechanical perspective, so far, very few studies have dealt with this topic. In most of the publications mentioned above, which deal with the mechanical characterisation of the SW, no reliable statements are made with regard to fibre orientations. Only Rotta et al. [63] indicate that fibres are aligned in circular and longitudinal directions, whereby this arrangement is irregular throughout the stomach. However, within this study, fibre orientation was measured by determining 6 histological in-plane images distributed over the height of the muscular layer, see IP1 to IP6 in Fig. 7(a). Results are illustrated in Fig. 8. Contrary to general statements that fibre orientation can be divided into three different sublayers by layer height, the data generated in this study revealed continuously changing orientations across the muscular layer, especially in the fundus. Here, the orientation changes from more longitudinal (outermost section) to a clear circumferential direction (innermost section). This continuously changing orientations is also visible in the corpus and antrum but is significantly less pronounced. However, after intensive literature research, only one study was found dealing with muscle fibre distribution in the muscle layer. In this study Birmingham [11], identified a three-layer (external, middle, internal) organisation of the muscular layer: In the external layer, the fibres are primarily oriented in the longitudinal direction, continuing with those of the oesophagus and the pylorus. In contrast, in the middle layer, fibres are primarily oriented in circular and oblique directions. Circumferential oriented fibres are numerous and are located across the entire stomach. In the fundus, near the oesophagus, the fibres become increasingly oblique. Finally, similar to the middle layer, for the internal layer, the authors identified circular and oblique oriented fibres, but in contrast to the middle layer, in the internal layer, the oblique oriented fibres prevailed. Basically, the results of [11] are consistent with those of the present study. The middle and internal layer findings are quite similar, whereby in the present study, more oblique oriented fibres were identified in the fundus.

Even if the layered microstructure of the SW is strongly inhomogeneous, cf. Fig. 7, the composition appears homogenous across the organ cf. Table 2.

### 4.3. Load transfer mechanisms in the stomach

One primary issue in understanding the mechanical behaviour of the SW that is also important for possible tissue engineered drafts for the stomach, is proper knowledge of load transfer mechanisms inside the SW. To analyse these load transfer mechanisms in detail, in Fig. 10, the region dependent, mean stress-stretch relationships in longitudinal and circumferential directions (0° sample orientation) for the intact SW, the muscular, and the mucosal layers are illustrated. At first glance, mechanical responses differ significantly between the various layers. This finding is surprising and contradictory to intuitive expectations and previous work [e.g. 33] showing that stresses of the intact SW represent an averaged stress state of the muscular and mucosal layers. Instead, stresses in the intact SW of the fundus (a) are higher for low and medium deformations until $\lambda \approx 1.4$ in both, longitudinal and circumferential direction. For the corpus and antrum, cf. (b) and (c), stresses in the intact SW are higher in the circumferential direction only for low values of $\lambda \approx 1.1$. However, a narrow range, where stresses in the intact SW represent the average stress of both layers separated, may exists in the fundus ($1.4 < \lambda < 1.5$), antrum ($1.1 < \lambda < 1.3$), and in the corpus ($1.0 < \lambda < 1.2$), respectively. For medium to large deformation, the stress-stretch relationship changes drastically. In the fundus, stresses in the mucosal layer increase much more

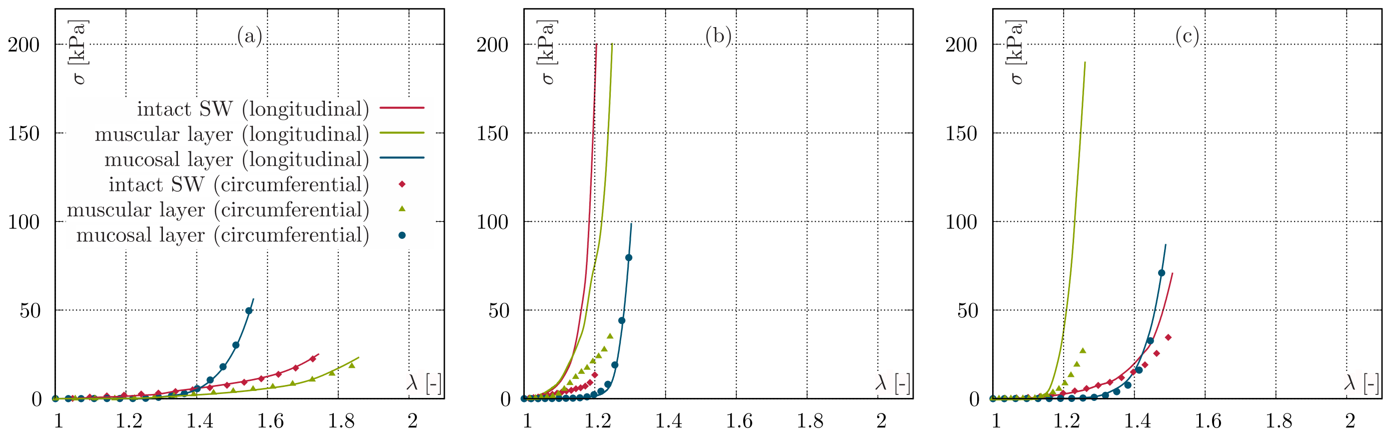


**Fig. 10.** Mean stress-stretch relations in longitudinal and circumferential direction (0° sample orientation) for the intact SW, the muscular, and the mucosal layers of the (a) fundus, (b) corpus, and (c) antrum.

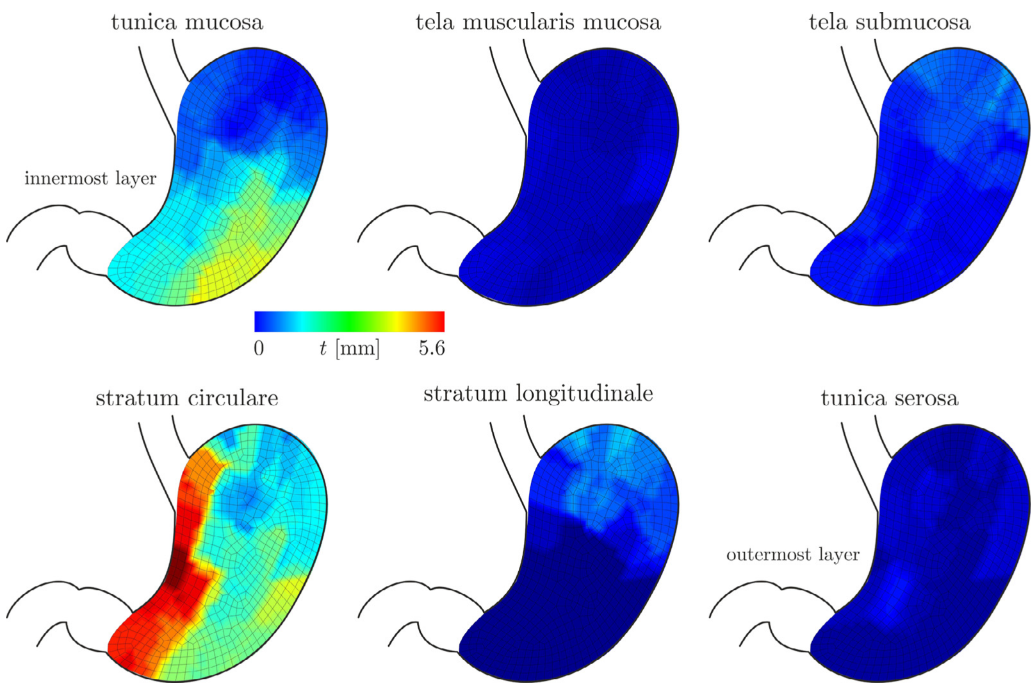


**Fig. 11.** Layer-specific stiffness distribution of the SW.

progressive than in the intact SW and muscle layer. On the other hand, in the antrum, the increase is similar in both layers, while in the corpus, the increase is comparable in both layers and the intact SW.

One possible explanation for this behaviour could be the influence of the interface between the layers on deformation modes of the muscle and mucosal layer during biaxial testing. Interestingly, such a deviation between the separated layers and the intact SW was not observed in previous work [33,76]. However, Zhao et al. [76] measured the lowest stress in the intact SW of the antrum. It was concluded that this was associated with the stiffness and thickness of the muscle layer, which is thickest in the antrum. However, there are two major differences between the experimental settings used in the referenced publications and in the present work: First, in the preceding works, samples were preconditioned, and second, for mechanical characterisation, uniaxial tension tests were applied.

Considering a fictitious case where both layers are isotropic and incompressible, the interface between the layers would not induce additional shear stresses. On the contrary, if the degree and orientation of anisotropy differs between the layers, additional shear stresses arise that constrain the natural deformation of the respective layer. As shown in Table 1, the measured shear deformations are very different between the separated layers and the intact SW. Herein, shear deformations are highest in the muscular layer, exhibiting values up to $\gamma_{\text{long}} = 0.38$ and $\gamma_{\text{circ}} = 0.46$ in the corpus. The least pronounced shearing was detected in the isotropic mucosal layer ($\gamma_{\text{long/circ}} < 0.1$). Unlike the stress-stretch relationship mentioned earlier in this section, shear deformations in the intact wall represent the average distortion of both layers attached to each other very well.

### *4.4. Functional aspects in relation to mechanical findings*

During digestion, the stomach has three primary motor functions: Storing, mixing, and emptying [26,38,48]. These functions occur in two distinct motor regions. While the proximal stomach (fundus and proximal corpus) takes responsibility for the storage of food intake, the distal stomach (distal corpus and antrum) is responsible for mixing and emptying [31]. The proximal stomach relaxes to receive the bolus from the oesophagus, where it is temporarily stored. Slow and sustained contractions press the gastric contents toward the distal stomach, emptying of liquids [35]. In the distal stomach, peristaltic contractions mix and grind the gastric contents until the solids are broken into sizes small enough (<1 mm) to pass through the pylorus [35].

We observed the highest thickness in the muscular layer, cf. Fig. 6, as well as almost exclusive circumferential muscle fibre orientation at the pyloric orifice (at the end of the antrum). This strong musculature allows the pylorus to remain closed while the gastric content is mixed and ground during antral recirculation [31,53].

The fundus comprises the most complex microstructure of the three stomach regions, see Fig. 7(a). Following Figs. 6 and 8, the muscular layer of the fundus is composed of two wavy layers (stratum circulare and stratum longitudinale) of variable thickness that feature different cross-orientations depending on their anatomical location. Mechanically, this microstructure allows the fundus to undergo large deformations with low stresses in all directions, see Fig. 5(a). Consequently, the fundus can dilate quickly to store ingested food, while keeping intragastric pressure low and acting as a reservoir [4,32]. The cross orientated muscle fibre structure of the fundus enables homogeneous deformation during contraction, promoting controlled transport of the bolus to the corpus. Furthermore, the fundus can resist elongations induced by contractions of the circumferential corpus and antrum muscular layers against the volume-constant (incompressible) gastric content.

The corpus and antrum exhibit more regular microstructure. The muscular layer thickens from the thinnest stomach region in the proximal corpus to the thick antrum, see Fig. 6(e). The smooth muscle fibre bundles run circumferentially perpendicular to the greater curvature, which makes the corpus and antrum behave such as an anisotropic material with a strong dependency on the orientation of the sample with respect to the testing axes, particularly in the corpus, see Fig. 5(d). These circumferential oriented fibre bundles are responsible for the peristaltic contractions that grind and crush food [38,66]. The thick mucosal layer aids in disintegration of large chunks of food during antral recirculation to produce a more liquid-like chyme with ongoing acid secretion [35,53].

### *4.5. Impact on stomach tissue engineering and stomach modelling*

For the first time, this study provides a comprehensive set of data that can be used to analyse and understand the complex load-transfer mechanisms within the SW. These data are of particular importance for tissue engineered materials [e.g. 5,27,28,46,59]. To develop artificial substitute material for the SW, it is important to understand the mechanical properties of all regions, how the fibres are distributed, which thickness distributions are present, and from which components the SW is composed. However, as it is demonstrated in Section 4.3, the underlying load transfer mechanisms at morphological and microstructural level are quite complex and in detail not understood. On the part of clinics, one is particularly interested in, not only in the case of the stomach, generating artificial tissue implants that assume the mechanical function of the tissue to be replaced in vivo [36,72]. At the microstructural level, the ECM is the decisive load transferring component [30]. Different methods such as electrospinning or three-dimensional printing are used to produce scaffolds, representing the ECM, which are overgrown will cells in the bioreactor [24,57]. However, studies on tissue engineering considering also morphological characteristics (e.g. waviness of the mucosal layer), as found within the present study, could not be found.

In addition to generally enhancing the physiological understanding of SW mechanics and its load transfer mechanisms, the present data may also be useful for the development of comprehensive, numerical models. To the best of the authors' knowledge, there exists no three-dimensional modelling approach describing the passive mechanical behaviour of the SW. The data and findings collected in this work are of particular importance for the development of three-dimensional models. Especially these type of information in form of histo-mechanical data motivates to model the SW as constrained mixture, see e.g. [10]. Such a model type is able to provide for individual constituents (here: SMC, ECM, and fat) different material properties and natural stress-free configurations. Thereby, the deformation is constrained and all constituents move together with the tissue.

## Declaration of Competing Interest

The authors declare that they have no known competing financial interests or personal relationships that could have appeared to influence the work reported in this paper.

## Acknowledgment

This work was supported by the Deutsche Forschungsgemeinschaft (DFG) under Grants BO 3091/18-1 and SI 841/12-1. The authors would like to thank Stephan Kohn, Philipp Steinke, and Juan Pablo Tenaglia for assisting in lab repetitive tasks necessary to conduct the study.

## Appendix A. Layer-specific thickness distributions

In Fig. 11 the thickness distributions for the single layers, namely (from inside to outside) tunica mucosa, tela muscularis mucosa, tela submucosa, stratum circulare, stratum longitudinale, and tunica serosa, are illustrated over the idealised stomach geometry, cf. also Remark 2. While the tela muscularis mucosa and the tunica serosa feature over all regions of the SW thicknesses close to zero, the tela submucosa and the stratum longitudinale exhibit higher thicknesses, especially in the fundus. The highest thicknesses and most inhomogeneous thickness distributions can be found in the tela mucosa and stratum circulare. Particularly in the area of the lesser curvature, the stratum circulare features the highest thickness. On the other side, in the area of the greater curvature the thickness is significantly smaller, substantiating the existence of a clear thickness gradient.

## Appendix B. Staining protocols

### *B.1. Picro-Sirius red staining protocol for porcine stomach wall*

1. Freeze the sample for 20 s in an isopentane bath cooled with liquid nitrogen.
2. Store the frozen sample wrapped in aluminum foil at −80 °C until use.
3. Cut sections 6 µm thick at −20 °C and put onto glass microscope slide.
4. Allow sections to precipitate at room temperature until the next day.
5. Fix sections with Picro-Formalin for 5 min.
6. Rinse sections under gently running water for 10 min.
7. Stain sections with Picro-Sirius red solution for 60 min.
8. Rinse sections with acidified water for 2 min 2 times.
9. Rinse sections with distilled water for 1 min.
10. Dehydrate sections with ethanol 96% for 1 min.
11. Dehydrate sections with isopropanol for 1 min 2 times.
12. Clear sections with Roti-Histol for 5 min.
13. Cover sections with a mounting medium.

### B.2. Elastica van Gieson staining protocol for porcine stomach wall

1. Freeze the sample for 20 s in an isopentane bath cooled with liquid nitrogen.
2. Store the frozen sample wrapped in aluminum foil at −80 °C until use.
3. Cut sections 6 µm thick at −20 °C and place onto a glass microscope slide.
4. Allow sections to precipitate at room temperature until the next day.
5. Rinse sections with ethanol 96%, ethanol 80% and ethanol 70% for 2 min each time.
6. Stain sections with Resorcinol Fuchsine for 15 min.
7. Rinse sections under gently running water for 10 min.
8. Stain sections with Van Gieson Picrofuchsine solution for 2 min.
9. Rinse sections with distilled water for 5 s.
10. Dehydrate sections with ethanol 96% for 2 min 2 times.
11. Dehydrate sections with isopropanol for 2 min.
12. Clear sections with Roti-Histol for 5 min 2 times.
13. Cover sections with mounting medium.

### B.3. Sudan III staining protocol for porcine stomach wall

1. Freeze the sample for 20 s in an isopentane bath cooled with liquid nitrogen.
2. Store the frozen sample wrapped in aluminum foil at −80 °C until use.
3. Cut Sections 6 µm thick at −20 °C and put onto glass microscope slide.
4. Allow sections to precipitate at room temperature until the next day.
5. Dehydrate sections with ethanol 96%, 80%, 70%, 60%, 50%, each for 2 minutes.
6. Stain sections with Sudan III for 5 min.
7. Rinse sections with ethanol 50% for 10 s.
8. Stain sections with Van Gieson Picrofuchsine solution for 2 min.
9. Rinse sections with distilled water for 2 min 2 times.
10. Cover sections with mounting medium.

## References


[1] G. Abdeen, C.W.L. Roux, Mechanism underlying the weight loss and complications of roux-en-y gastric bypass. review, Obes. Surg. 26 (2) (2016) 410–421.
[2] N.K. Ahluwalia, D.G. Thompson, J. Barlow, L.E. Troncon, S. Hollis, Relaxation responses of the human proximal stomach to distension during fasting and after food, Am. J. Physiol. 267 (2) (1994) G166–G172.
[3] N.R. Akhmadeev, R. Miftahof, Stress-strain distribution in the human stomach, Int. J. Des. Nat.Ecodyn. 5 (2) (2010) 90–107.
[4] T. Arakawa, H. Uno, T. Fukuda, K. Higuchi, K. Kobayashi, T. Kuroki, New aspects of gastric adaptive relaxation, reflex after food intake for more food: involvement of capsaicin-sensitive sensory nerves and nitric oxide, J. Smooth Muscle Res. 33 (3) (1997) 81–88.
[5] M. Araki, H. Tao, T. Sato, N. Nakajima, S.H. Hyon, T. Nagayasu, T. Nakamura, Development of a new tissue-engineered sheet for reconstruction of the stomach, Artif. Organs 33 (10) (2009) 818–826.
[6] R.C. Aydin, S. Brandstaeter, F.A. Braeu, M. Steigenberger, R.P. Marcus, K. Nikolaou, M. Notohamiprodjo, C.J. Cyron, Experimental characterization of the biaxial mechanical properties of porcine gastric tissue, J. Mech. Behav. Biomed. Mater. 74 (2017) 499–506.
[7] F. Azpiroz, J.R. Malagelada, Physiological variations in canine gastric tone measured by an electronic barostat, Am. J. Anat. 248 (2) (1985) G229–G237.
[8] F. Azpiroz, J.R. Malagelada, Gastric tone measured by an electronic barostat in health arid postsurgical gastroparesis, Gastroenterology 92 (4) (1987) 934–943.
[9] L. Berbiglia, J.G. Zografakis, A.G. Dana, Laparoscopic roux-en-y gastric bypass: surgical technique and perioperative care, Surg. Clin. North Am. 96 (4) (2016) 773–794.
[10] C. Bellini, J. Ferruzzi, S. Roccabianca, E.S.D. Martino, J.D. Humphrey, A microstructurally motivated model of arterial wall mechanics with mechanobiological implications, Ann. Biomed. Eng. 42 (3) (2014) 488–502.
[11] A. Birmingham, The arrangement of the muscular fibres of the stomach, Trans. R. Acad. Med.Irel. 16 (1) (1898) 432–440.
[12] R.L.A.W. Bleys, T.J. Weijs, Surgical anatomy of esophagus, in: M.A. Cuesta (Ed.), Minimally Invasive Surgery for Upper Abdominal Cancer, Springer International Publishing, Cham, 2017, pp. 11–20.
[13] J.S. Bolton, W.C. Conway, Postgastrectomy syndromes, Gastric Surg. 91 (5) (2011) 1105–1122.
[14] M. Borsdorf, A. Tomalka, N. Stutzig, E.M. Orcajo, M. Böl, T. Siebert, Locational and directional dependencies of smooth muscle properties in pig urinary bladder, Front. Physiol. 10 (2019) 63.
[15] S. Brandstaeter, S.L. Fuchs, R.C. Aydin, C.J. Cyron, Mechanics of the Stomach: A Review of an Emerging Field of Biomechanics, GAMM-Mitteilungen, 2019, pp. 1–17. ISSN 0936-7195.
[16] F. Bray, J. Ferlay, I. Soerjomataram, R.L. Siegel, L.A. Torre, A. Jemal, Global cancer statistics 2018: globocan estimates of incidence and mortality worldwide for 36 cancers in 185 countries, Cancer J. Clin. 68 (6) (2018) 394–424.
[17] E.L. Carniel, A. Frigo, C.G. Fontanella, G.M. de Benedictis, A. Rubini, L. Barp, G. Pluchino, B. Sabbadini, L. Polese, A biomechanical approach to the analysis of methods and procedures of bariatric surgery, J. Biomech. 56 (2017) 32–41.
[18] J.L. Davis, R.T. Ripley, Postgastrectomy syndromes and nutritional considerations following gastric surgery, Gastric Surg. 97 (2) (2017) 277–293.
[19] P. Du, G. O'Grady, J.B. Davidson, L.K. Cheng, A.J. Pullan, Multiscale modeling of gastrointestinal electrophysiology and experimental validation, Crit. Rev. Biomed. Eng. 38 (3) (2010) 225–254.
[20] J.C. Eagon, K.A. Kelly, B.W. Miedema, Postgastrectomy syndromes, Gastric Surg. 72 (2) (1992) 445–465.
[21] V.I. Egorov, I.V. Schastlivtsev, E.V. Prut, A.O. Baranov, R.A. Turusov, Mechanical properties of the human gastrointestinal tract, J. Biomech. 35 (10) (2002) 1417–1425.
[22] C.G. Fontanella, C. Salmaso, I. Toniolo, N. de Cesare, A. Rubini, G.M. de Benedictis, E.L. Carniel, Computational models for the mechanical investigation of stomach tissues and structure, Ann. Biomed. Eng. (2019).
[23] H. Gregersen, O.H. Gilja, T. Hausken, A. Heimdal, C. Gao, K. Matre, S. Ødegaard, A. Berstad, Mechanical properties in the human gastric antrum using b-mode ultrasonography and antral distension, Am. J. Physiol. 283 (2) (2002) G368–G375.
[24] Y. Greish, S.M. Karam, A.H.I. Mourad, S. Pulikkot, Biodegradable scaffolds for gastric tissue regeneration, Scaffolds in Tissue Engineering-Materials, Technologies and Clinical Applications. IntechOpen, 2017.
[25] T. Grikscheit, A. Srinivasan, J.P. Vacanti, Tissue-engineered stomach: a preliminary report of a versatile in vivo model with therapeutic potential, J. Pediatric Surg. 38 (9) (2003) 1305–1309.
[26] A.R. Hobson, Q. Aziz, Oesophagus and stomach motility, Medicine 39 (4) (2011) 210–213. ISSN 1357-3039
[27] Y. Hori, T. Nakamura, K. Matsumoto, Y. Kurokawa, S. Satomi, Y. Shimizu, Experimental study on in situ tissue engineering of the stomach by an acellular collagen sponge scaffold graft, Am. Soc. Artif. Intern. Organs 47 (3) (2001) 206–210.
[28] Y. Hori, T. Nakamura, D. Kimura, K. Kaino, Y. Kurokawa, S. Satomi, Y. Shimizu, Functional analysis of the tissue-engineered stomach wall, Artif. Organs 26 (10) (2002) 868–872.
[29] B.T. Horton, Pyloric musculature, with special reference to pyloric block, Am. J. Anat. 41 (2) (1928) 197–225.
[30] G.S. Hussey, M.C. Cramer, S.F. Badylak, Extracellular matrix bioscaffolds for building gastrointestinal tissue, Cellular and Molecular Gastroenterology and-Hepatology 5 (1) (2017) 1–13. ISSN 2352-345X
[31] Y. Imai, I. Kobayashi, S. Ishida, T. Ishikawa, M. Buist, T. Yamaguchi, Antral recirculation in the stomach during gastric mixing, Am. J. Physiol. 304 (5) (2013) G536–G542.
[32] P. Janssen, S. Verschueren, H.G. Ly, R. Vos, L. van Oudenhove, J. Tack, Intragastric pressure during food intake: a physiological and minimally invasive method to assess gastric accommodation, Neurogastroenterol. Motil. 23 (4) (2011) 316–e154.
[33] Z.G. Jia, W. Li, Z.R. Zhou, Mechanical characterization of stomach tissue under uniaxial tensile action, J. Biomech. 48 (4) (2015) 651–658.
[34] A.D. Keet, The Pyloric Sphincteric Cylinder in Health and Disease, Springer Science & Business Media, 1993.
[35] K.A. Kelly, Gastric emptying of liquids and solids: roles of proximal and distal stomach, Am. J. Physiol. 239 (2) (1980) G71–G76.
[36] I.G. Kim, Y. Wu, S.A. Park, H. Cho, J.J. Choi, S.K. Kwon, J.W. Shin, E.J. Chung, Tissue-engineered esophagus via bioreactor cultivation for circumferential esophageal reconstruction, Tissue Eng. Part A (2019).
[37] B. Kmiecik, A. Skotny, J. Detyna, Structure and mechanical properties of soft tissues during selected pathological processes, J. Blood Disord. Transfus. 5 (2017).
[38] F. Kong, R.P. Singh, Disintegration of solid foods in human stomach, J. Food Sci. 73 (5) (2008) R67–R80.
[39] S. Korossis, F. Bolland, J. Southgate, E. Ingham, J. Fisher, Regional biomechanical and histological characterisation of the passive porcine urinary bladder: implications for augmentation and tissue engineering strategies, Biomaterials 30 (2) (2009) 266–275.
[40] D. Liao, J. Zhao, H. Gregersen, Regional surface geometry of the rat stomach based on three-dimensional curvature analysis, Phys. Med. Biol. 50 (2) (2005) 231–246.
[41] D. Liao, J. Zhao, H. Gregersen, A novel 3d shape context method based strain analysis on a rat stomach model, J. Biomech. 45 (9) (2012) 1566–1573.
[42] C.E. Mackintosh, L. Kreel, Anatomy and radiology of the areae gastricae, Gut 18 (11) (1977) 855–864. ISSN 1458-3288

[43] T. Maemura, M. Shin, M. Sato, H. Mochizuki, J.P. Vacanti, A tissue-engineered stomach as a replacement of the native stomach, Transplantation 76 (1) (2003) 61–65. ISSN 0041-1337
[44] T. Maemura, K. Ogawa, M. Shin, H. Mochizuki, J.P. Vacanti, Assessment of tissue-engineered stomach derived from isolated epithelium organoid units, Transplant. Proc. 36 (5) (2004) 1595–1599.
[45] T. Maemura, M. Shin, O. Ishii, H. Mochizuki, J.P. Vacanti, Initial assessment of a tissue engineered stomach derived from syngeneic donors in a rat model, Am. Soc. Artif. Intern. Organs 50 (5) (2004) 468–472.
[46] T. Maemura, M. Shin, M. Kinoshita, Tissue engineering of the stomach, J. Surg. Res. 183 (1) (2013) 285–295.
[47] V. Mahadevan, Anatomy of the stomach, Surgery 32 (11) (2014) 571–574.
[48] V. Mahadevan, Anatomy of the stomach, Surgery 35 (11) (2017) 608–611.
[49] R.N. Miftahof (Ed.), Biomechanics of the Human Stomach, Springer, 2017.
[50] J. Miller, G. Kauffman, J. Elashoff, H. Ohashi, D. Carter, J.H. Meyer, Search for resistances controlling canine gastric emptying of liquid meals, Am. J. Physiol. 241 (5) (1981) G403–G415.
[51] E. Morales-Orcajo, T. Siebert, M. Böl, Location-dependent correlation between tissue structure and the mechanical behaviour of the urinary bladder, Acta Biomater. 75 (2018) 263–278.
[52] J. Nagatomi, D.C. Gloeckner, M.B. Chancellor, W.C. de Groat, M.S. Sacks, Changes in the biaxial viscoelastic response of the urinary bladder following spinal cord injury, Ann. Biomed. Eng. 32 (10) (2004) 1409–1419.
[53] A. O'Connor, C. O'Moráin, Digestive function of the stomach, Digestive Diseases 32 (3) (2014) 186–191. ISSN 0257-2753
[54] O. College, The digestive system, Anat. Physiol. (2013).
[55] D.A. Owen, Normal histology of the stomach, Am. J. Surg. Pathol. 10 (1) (1986) 48–61.
[56] A. Parekh, A.D. Cigan, S. Wognum, R.L. Heise, M.B. Chancellor, M.S. Sacks, Ex vivo deformations of the urinary bladder wall during whole bladder filling: contributions of extracellular matrix and smooth muscle, J. Biomech. 43 (9) (2010) 1708–1716.
[57] S.Y. Park, J.W. Choi, J.K. Park, E.H. Song, S.A. Park, Y.S. Kim, Y.S. Shin, C.H. Kim, Tissue-engineered artificial oesophagus patch using three-dimensionally printed polycaprolactone with mesenchymal stem cells: a preliminary report, Interact. Cardiovasc. Thor. Surg. 22 (6) (2016) 712–717.
[58] H.P. Parkman, M.P. Jones, Tests of gastric neuromuscular function, Gastroenterology 136 (5) (2009) 1526–1543.
[59] R.A. Penkala, S.S. Kim, Gastrointestinal tissue engineering, Expert Rev. Med. Dev. 4 (1) (2007) 65–72.
[60] C. Penning, M.K. Vu, J.B. Delemarre, A.A. Masclee, Proximal gastric motor and sensory function in slow transit constipation, Scand. J. Gastroenterol. 36 (12) (2001) 1267–1273.
[61] R. Rezakhaniha, A. Agianniotis, J.T.C. Schrauwen, A. Griffa, D. Sage, C.V.C. Bouten, F.N. van de Vosse, M. Unser, N. Stergiopulos, Experimental investigation of collagen waviness and orientation in the arterial adventitia using confocal laser scanning microscopy, Biomech. Model. Mechanobiol. 11 (3) (2012) 461–473.
[62] J. Rosen, J.D. Brown, S. De, M. Sinanan, B. Hannaford, Biomechanical properties of abdominal organs in vivo and postmortem under compression loads, J. Biomech. Eng. 130 (2) (2008) 021020–021020–17.
[63] G. Rotta, J. Kobiela, S. Grymek, M. Karczewska, Mechanical properties of the human stomach under uniaxial stress action, Curr. Sci. 116 (11) (2019) 1886.
[64] K. Schulze, Imaging and modelling of digestion in the stomach and the duodenum, Neurogastroenterol. Motil. 18 (3) (2006) 172–183.
[65] K. Schulze-Delrieu, R.J. Herman, S.S. Shirazi, B.P. Brown, Contractions move contents by changing the configuration of the isolated cat stomach, Am. J. Physiol. 274 (2) (1998) G359–G369.
[66] W. Schwizer, A. Steingoetter, M. Fox, Magnetic resonance imaging for the assessment of gastrointestinal function, Scand. J. Gastroenterol. 41 (11) (2006) 1245–1260.
[67] M. Sharma, P. Rai, C.S. Rameshbabu, B. Senadhipan, Imaging of peritoneal ligaments by endoscopic ultrasound (with videos), Endosc. Ultrasound 4 (1) (2015) 15–27.
[68] G. Sommer, A. Schriefl, G. Zeindlinger, A. Katzensteiner, H. Ainödhofer, A. Saxena, G.A. Holzapfel, Multiaxial mechanical response and constitutive modeling of esophageal tissues: Impact on esophageal tissue engineering, Acta Biomater. 9 (12) (2013) 9379–9391.
[69] G. Sommer, D.C. Haspinger, M. Andrä, M. Sacherer, C. Viertler, P. Regitnig, G.A. Holzapfel, Quantification of shear deformations and corresponding stresses in the biaxially tested human myocardium, Ann. Biomed. Eng. 43 (10) (2015) 2334–2348.
[70] W. Sun, M.S. Sacks, M.J. Scott, Effects of boundary conditions on the estimation of the planar biaxial mechanical properties of soft tissues, J. Biomech. Eng. 127 (4) (2005) 709–715.
[71] A. Tomalka, M. Borsdorf, M. Böl, T. Siebert, Porcine stomach smooth muscle force depends on history-effects, Front. Physiol. 8 (2017) 802.
[72] M.J. Webber, O.F. Khan, S.A. Sydlik, B.C. Tang, R. Langer, A perspective on the clinical translation of scaffolds for tissue engineering, Ann. Biomed. Eng. 43 (3) (2015) 641–656.
[73] R.L. Wilson, C.E. Stevenson, C.J. Yeo, Chapter 56 - anatomy and physiology of the stomach, in: Shackelford's Surgery of the Alimentary Tract, 2 Volume Set (Eighth Edition), 2019, pp. 634–646. Philadelphia
[74] S. Wognum, D.E. Schmidt, M.S. Sacks, On the mechanical role of de novo synthesized elastin in the urinary bladder wall, J. Biomech. Eng. 131 (10) (2009) 1–11.
[75] J. Zhao, D. Liao, H. Gregersen, Tension and stress in the rat and rabbit stomach are location- and direction-dependent, Neurogastroenterol. Motil. 17 (3) (2005) 388–398.
[76] J. Zhao, D. Liao, P. Chen, P. Kunwald, H. Gregersen, Stomach stress and strain depend on location, direction and the layered structure, J. Biomech. 41 (16) (2008) 3441–3447.